Synthesis and Characterization of Self-Assembling Amphiphiles for a Targeted Drug Delivery System to Treat Pancreatic and Colon Cancer

Honors Research Thesis

Presented in Partial Fulfillment of the Requirements for graduation
"with Honors Research Distinction in Chemistry" in the undergraduate
colleges of The Ohio State University

by
Samantha King

The Ohio State University
March 2013

Project Advisor: Dr. Jon R. Parquette, Department of Chemistry

Abstract

Cancer is becoming an ever-growing focus of the medical and research fields with regards to treatment and elimination. Pancreatic cancer is the fourth leading cause of death in the United States due to the difficulty in detection and treatment. The current survival rate over five years is 4%. Many possible treatments for pancreatic cancer currently exist; however, is difficult to deliver large amount of toxic cancer drugs to targeted tumor sites without significant and often deadly side effects for patients. Nanometer-scale drug delivery vehicles have proven to be one advantageous method to reduce drug toxicity. The goal of this project is to explore the use of self-assembling nanotubes based on peptide-camptothecin derivatives to allow for increased targeting of cancer cells during the course of treatment. Three compounds were formed from camptothecin, succinic acid and lysine derivatives- lysine methyl ester, lysine, lysine amide. They were tested in water and phosphate buffer solution (PBS), mimicking biological conditions, for their solubility and ability to self-assemble into specific and stable aggregates. The soluble compounds were tested and imaged for confirmation of nanostructures and identification of self-assembly process via transmission electron microscopy and circular dichroism scans. The methyl ester form (**1.0**) created nanotubes in water while the free acid form (**2.0**) and amide form (**3.0**) created nanotubes in PBS. The potential for a dynamic system was tested but modifications to the design must be made to take advantage of this characteristic and perfect the drug delivery system.

Acknowledgements

First and foremost, I would like to thank my research advisor, Dr. Jon R. Parquette, for giving me the opportunity to join his group and perform research in his lab over the last few years. He has spent much time on an endless number of occasions answer questions pertaining to research, organic chemistry as well as a variety of other subjects. He helped me to develop the skills I needed to conduct organic chemistry research and the skills critically solve problems.

I would like to thank the Beckman Research Institute and the Ohio State University Department of Chemistry for their financial and creative support of this project; I would not have had the same experience without the support.

I would also like to thank Jacob Dumbleton for all of his help in starting research, beginning my project and during my time in lab in general. He answered numerous amounts of questions, taught me the basics of lab and organic chemistry before I took any classes and I would not have completed this project without his help.

I would like to thank Se Hye Kim for her knowledge and help with this project. Her guidance helped me troubleshoot many obstacles that I otherwise may not have overcome. Also, her help in imaging and interpreting data was invaluable. I would also like to thank Kwang Soo (Patrick) Lee with his help in running the CD/UV scans. I would also like to thank the other members of the lab for their help and answering my boatload of questions about reactions and locations of chemicals and the like.

And finally I want to thank my friends and family for all of their support. I appreciate them listening to my rambles, my frustration and for celebrating my successes. I know my rants were often a mess of scientific terms that often made their eyes glaze over but their support allowed me to continue my research. Thank you!

Table of Contents

Abbreviations:

Alloc: allyloxycarbonyl

Boc: tert-butyloxycarbony

Chloro-trityl resin: 2-Chlorotrityl chloride resin

CPT: camptothecin

DBU: 1,8-Diazabicyclo[5.4.0]undec-7-ene

DCM: dichloromethane

DMAP: 4-Dimethylaminopyridine

DMF: dimethylformamide

EDCI: 1-Ethyl-3-(3-dimethylaminopropyl)carbodiimide

Fmoc: fluorenylmethyloxycarbonyl

HOBt: Hydroxybenzotriazole

Lys: lysine

MeOH: methanol

NMM: N-Methylmorpholine

THF: tetrahydrofuran

TIS: Triisopropylsilane

Wang Resin: p-Benzyloxybenzyl alcohol resin

Z: Benzyloxy-carbonyl

1. Introduction

Pancreatic carcinoma, of all types of cancers, has proven to be one of the hardest to diagnose and treat.[1] Diagnosis for pancreatic cancer often does not occur until later stages when the tumor has metastasized and spread to a point where classic treatment methods are no longer viable.[2] This late detection is due to a lack of symptoms and difficulty in detection as the pancreas lies under other major organs.[2] Survival rates for pancreatic cancer are less than 5% over five years after diagnosis. Colorectal cancer is the third most commonly diagnosed cancer among men and women and in 2012 accounted for 9% of cancer deaths in the United States.[3] Depending on the origin of the colon cancer, survival rates for five years can vary from as high as 90% for cancer developing from polyps to lower than 30% for undifferentiated carcinoma, small cell carcinoma, signet ring cell carcinoma, and melanoma histologic groups.[4] When detected at an early stage the survival rate for colon cancer is 90% but only 39% of cases are diagnosed at that stage.[3] The survival rate dips down to 58% for 10 years, and continues to decrease from that survival rate.[3] With these potential low outcomes for colon cancer and extremely low outcomes for pancreatic cancer, there is great need for improved treatment methods. Current methods of treatment include surgery, chemotherapy and a combination of the two.

Surgery has played a key role in the treatment of the pancreatic carcinoma in the past, as well as other types of cancers such as breast cancer, because the disease has largely drug resistant. Although removing the tumor can increase survival, local reoccurrence occurs in 85% of patients who undergo surgery alone for treatment.[5] Also, not all patients diagnosed have resectable, non-metastatic tumors, 80% of patients generally have non-resectable advanced or metastatic tumors.[6] Surgery alone is not a sufficient treatment for pancreatic cancer.[7] A

combination of surgery and radiation improves the survival times and quality of life; but, it still has a low survival rate with some patients showing a 0% response rate.[2] While a combination of surgery and chemotherapy is the most likely source of progress in treatment, new drug therapies are needed for improved outcomes.[5]

Surgery has often proved successful for colorectal cancer but usually requires a combination with chemotherapy to fully eradicate the cancer.[3] It is the most common treatment for this type of cancer and proves successful when the tumor can be removed.[3] However, for ultimate success, the treatment with chemotherapy both pre- and post-surgery is required rather than surgery alone.[3] This treatment is where improvements can be made.

There are a variety of drugs currently available for treatment and eradication of pancreatic cancer in patients. A common issue with many of them is the uniquely high resistance of pancreatic cancer and the extreme toxicity of the drugs. The currently preferred drug choice is gemcitabine though it has had a low response rate and still unfavorable survival rates. Gemcitabine has been combined with other drugs like Erlotinib and Bevacizumab in an attempt to improve outcomes.[8,9] Though the use of combination therapies may provide a new pathway to increased survival, such methods lead to increased toxicity, which in turn causes complications such as bleeding, thrombosis and hypertension.[9] There are other compounds, such as Sansalvamide A derivatives, that are being tested that have equivalent survival rates as current methods but do not show improvement. However, current methods of treatment have dismal survival rates.[10] Gemcitabine is the only drug that can be considered as a first-line therapy for treatment, though it has a minimal effect on survival and in trials nearly half the patients required hospitalization for toxicity from the treatments.[5]

Chemotherapeutic treatment for colorectal patients include monoclonal antibody therapies currently approved by the FDA.[3] These drugs are Bevacizumab, which blocks the growth of blood vessels to the tumor, and Cetuximab and Panitumumab which both block the effects of the hormone-like factors that promote cancer growth.[3] However, chemotherapy as a treatment is limited by the toxicity of the drugs which may prevent the required dose from being given, especially to patients over the age of 70.[3] This type of treatment is effective when the cancer has not spread and can easily be removed, but colorectal cancer has the possibility of spreading to other vital organs, which can decrease treatment effectiveness and survival rates greatly.[4]

Nanosomes, nanospheres, nanotubes and other nanoparticles have all been used for the delivery of anti-cancer agents, incorporating drugs that have been too toxic or too difficult to deliver previously.[11] Studies done comparing the uses of the various structures and forms show that some forms are more favorable.[11] Stabilized structures work better than non-stabilized, defined structures are more effective than random aggregates, and encapsulated drugs show less toxicity than non-encapsulated structures when creating treatments for cancer therapies.[11] These structures provide a potentially safe and more efficacious method of delivery.[11] More research is needed to show the mechanism by which these nanostructures work, but their efficacy has been shown.

Nanotubes are functional, technological developments that provide a variety of structure types, uses, and features. They can naturally occur at all scales and play important roles in biology, such as micelles, for intracellular and extracellular transport, and tubulin.[12] Nanostructures for biological function can self-assemble with the aid of enzymes or for our purpose without the aid of enzymes.[12-13] Nanotubes and other nanostructures have been used for

various purposes such as detecting the activity of enzymes, controlling the fates of cells, and developing drug delivery systems. [12] Therefore self-assembling nanotubes provide a promising basis for a targeted drug delivery system, as other nanostructures have been implemented for various biological uses both naturally and artificially.[12]

The basis for using nanostructures is both to protect the encapsulated drug as well as to exploit the enhanced permeability and retention effect (EPR) to accumulate the pro-drug in tumor tissues. As tumors grow at an accelerated rate, they must provide a sufficient supply of oxygen and nutrients to maintain their growth. These newly formed tumor vessels grow in abnormal form and have a defective structure, which leads to enhanced vascular permeability, large gaps form in between endothial cells allowing for the entrance of nanoscale molecules.[14, 15, 16] It has been observed that particles on the scale of 10-100 nm accumulate in tumor tissues due to the leaky vasculature nature of blood vessels surrounding tumor tissues.[15] Nanoparticles, such as gold particles, carbon nanotubes, and more, have shown promise for the development of novel cancer diagnostic techniques and have the ability to enter tumor sites due to the EPR effect and the high O_2 demand in contrast with healthy tissue because of their increased growth rates.[17,18,19] But these current particles have difficulty in controlling size and surface chemistry. Also, these structures show a high potential for toxicity in humans, which limits drug development and creating models for delivery.[20,21] While pancreatic cancer has shown decreased vasculature in metastatic tumors, creating a hypertensive state or use of angiotensin II can augment the EPR effect in hypovascular tumors with minimal effect on normal tissue when the augmenting drugs are administered simultaneously with the treatment.[22]

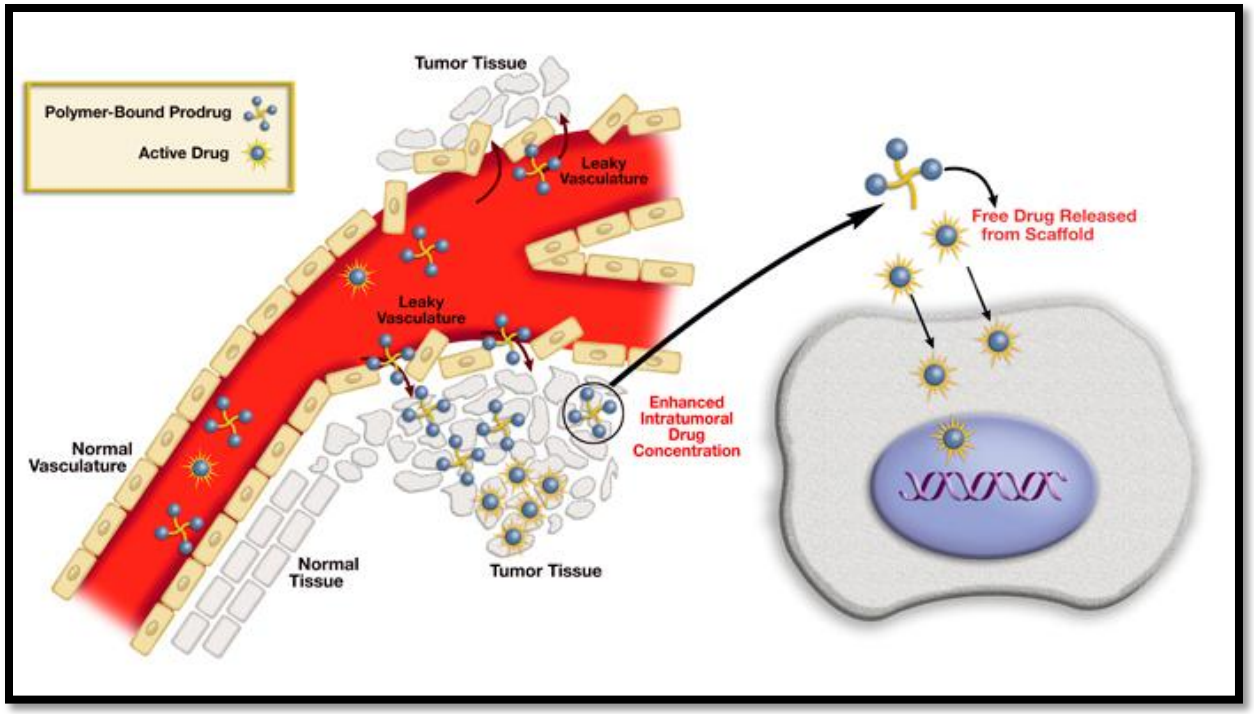

Figure. 1 Enhanced permeability and retention effect[23]

Camptothecin is one of the many drugs that have been investigated to use as a treatment for a broad range of cancer cells.[24] Its mode of action is through the inhibition of topoisomerase I which results in DNA strand breakage during replication thus leading to cell apoptosis.[24] However, in its natural form it is highly toxic and lethal in quantities needed for remission.[24] The other issue with camptothecin is that its natural form is insoluble in water, a property necessary for infusion treatment. Also, the key portion of camptothecin is the lactone (E-ring) portion of the drug that at physiological pH tends toward the open carboxylic form, rendering the drug inactive.[25] Albumin proteins in the blood also bind to the camptothecin and can render it inactive.[25] However, soluble derivatives of this compound, such as topotecan and irinotecan, have shown some tolerability and activity against various types of tumors such as small cell lung cancer, breast cancer, and in cell lines where other drugs have encountered resistance.[24] Camptothecin, if modifications can be made to increase solubility, has potential for efficacious

treatment for pancreatic cancer if the toxicity can be kept at a minimum and targeting of a modified form can be increased.[24]

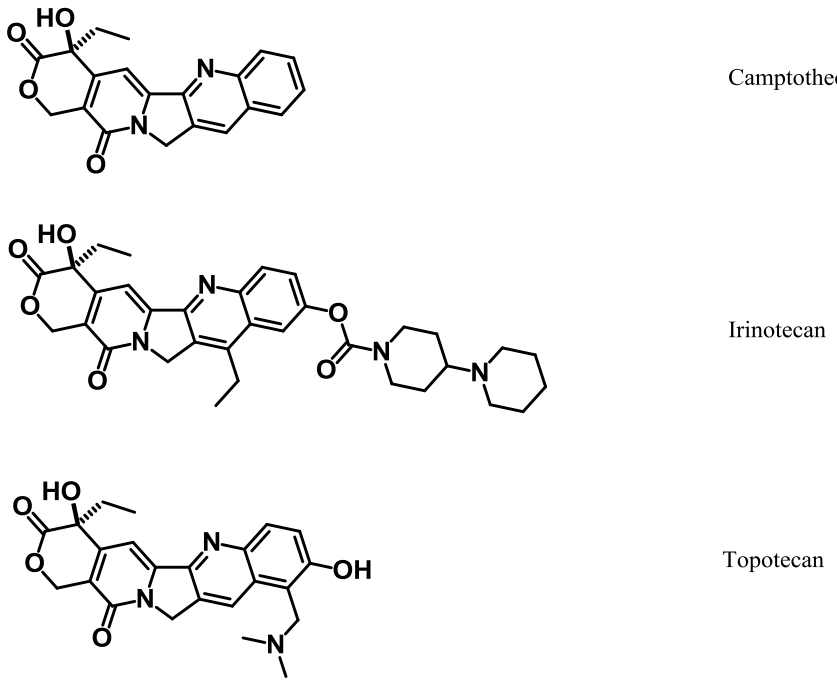

Figure 1.2. Camptothecin and Modified forms

The Parquette lab at the Ohio State University has developed self-assembling nanostructures, without the aid of enzymes for various purposes. These structures include nanotubes, fibers, spheres and random aggregates with a focus on creating organized structures. The nanotubes self-assemble due to their amphiphilic properties.[26] Within the peptide-dendron model created,the hydrophilic lysine and the hydrophobic NDI cause the compounds to self-assemble into nanotubes in an aqueous environment.[26] Organized structures have been shown to be more effective for drug delivery systems and tend to increase stability.[11] One of the worries with toxic cancer drugs like camptothecin is the threat of death to other cells in the body. Exploiting the EPR effect will allow for cancer cells to be targeted where as normal cells and tissue, which do not exhibit leaky vasculature, will remain unaffected.[16] Therefore, allowing for an increase in drug dosage without the toxic effects that are typically seen when giving high

doses of campothecin, and the standard treatment gemcitabine. Placing the highly toxic drugs in peptide based nanoparticles can reduce their toxicity but increase their efficacy.[11] When placed in large cyclodextrin-based polymer structures, the camptothecin conjugate shows increased tumor activity when compared to campothecin alone, or modified form, irinotecan. [24,27,28] Amphiphilic cyclodextrin models have also shown increased drug dosing and antitumor activity when compared with modified camptothein forms and other nanoparticle models.[29]

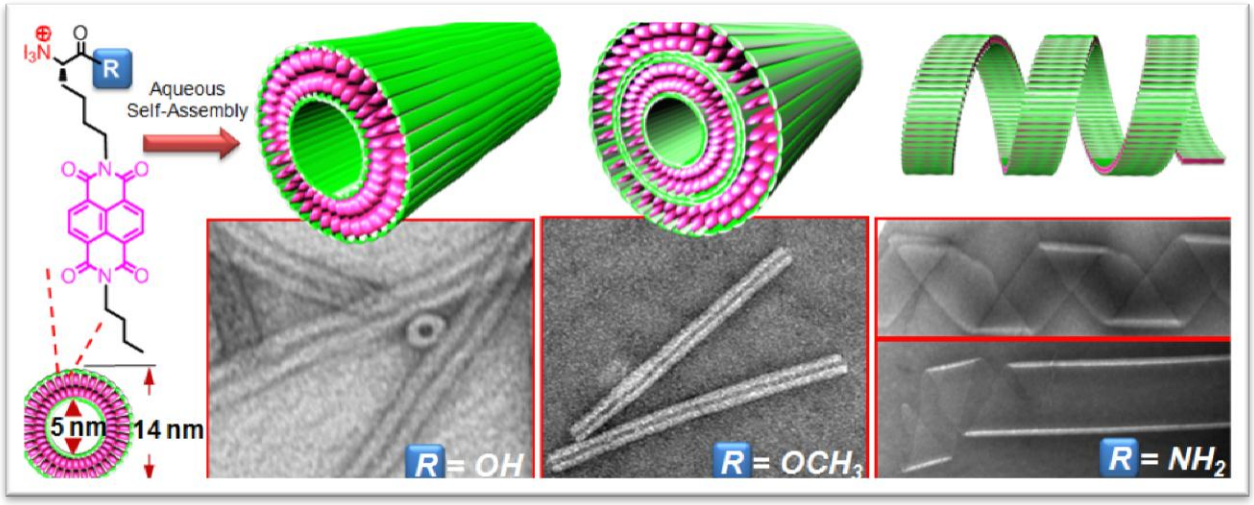

Figure 1.3. Hui Shao's model and image of nanotubes created using the peptide-dendron model.

Another feature of the nanotubes model is the potential for a dynamic system. A dynamic system means one where the nanostructure of a compound in solution can be changed by changing the solution components, for example pH, salt concentration and activity of solution. This system is different from many carbon nanotubes and other inorganic systems which create rigid and unchanging structures. As a tumor produces a different environment than exists in the blood, a dynamic system if designed correctly could allow for an easy release of the drug by hydrolysis once the nanotube enters the tumor, therefore maintaining targeting and increased chance of delivery.[30]

The objective of this project is to create a self-assembling nanotube system that incorporates camptothecin. The goal is for the compound to be soluble in phosphate buffer solution (PBS), a mimic for human blood that is suitable for testing conditions, and to form nanotubes that encapsulate the drug and are within 10-100 nm to allow to exploitation of the EPR effect. The current design for targeted drug delivery nanotubes is based on of the NDI-lysine model. Lysine methyl ester will be used for the hydrophilic portion of the compound and camptothecin, a nearly flat aromatic (similar structure is found in NDI) will be used for the hydrophobic portion. These two pieces will be connected by succinic acid. By mimicking the NDI-lysine model, the compounds are likely to form assemblies with the camptothecin encapsulated, as was discussed a key feature of success for drug delivery systems.[11] Because of the hydrophilic lysine, the nanotubes, like their predecessors will be soluble in water, a key feature for intravenous medicine. The compound will be made up of lysine methyl ester, succinic acid and camptothecin. Besides the toxic cancer drug, this compound uses compounds that naturally occur in the body, lysine being a natural amino acid and succinic acid also found in vivo and used in the Kreb's cycle. Thus the only damaging feature is the camptothecin, which will theoretically only be in the cancer cells. The nanotubes by design can also be opened up inside the cells by hydrolysis if the ester linkage and the non-cancer drug parts can easily be handled by the cells. The proposed structure includes necessary key features as denoted by past studies while incorporating innovative ideas for increasing the efficacy of the delivery system.

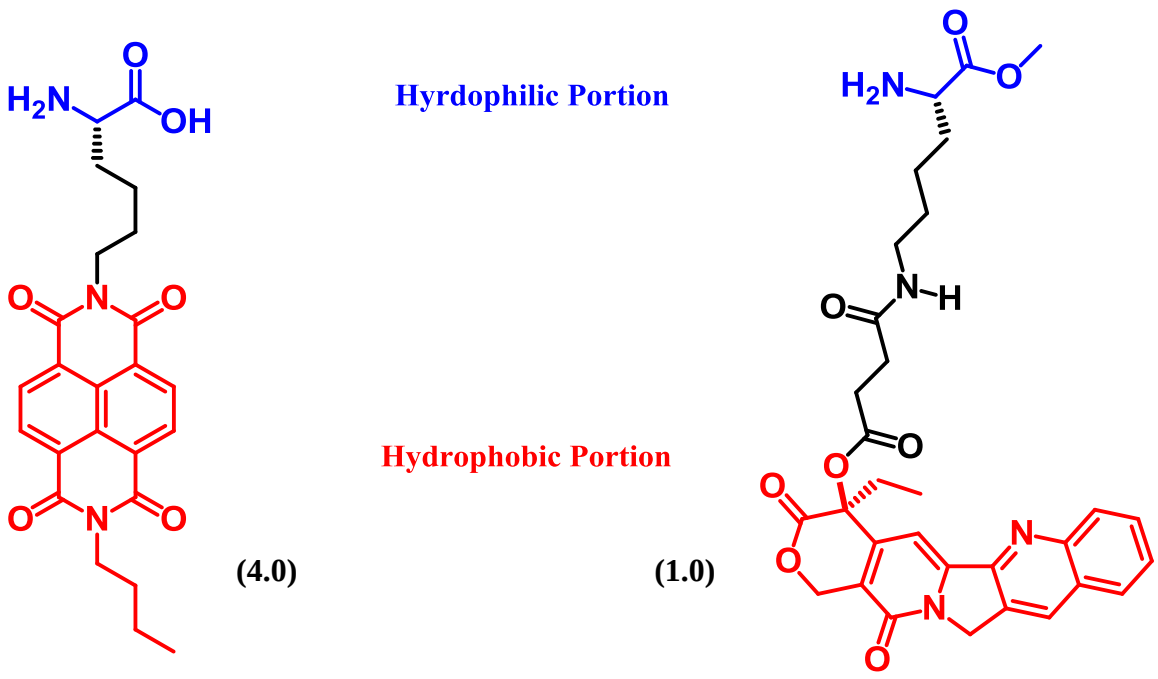

Figure 1.4. Comparison of semi-conductor model with cancer drug model

Compound **1.0** was synthesized in solution based reactions. The compound was then tested for solubility and nanostructure formation through circular dichroism scans, transmission electron microscopy. Compounds **2.0** and **3.0** were created on resin, cleaved and underwent similar testing methods. Compound **1.0** was then tested to determine if the structures were maintained when the nanostructure was formed in one solution and then placed in another solution, potential for dynamic system.

Various nanostructures were created based on composition of the solvent as well as various changes to the polar head, hydrophilic portion, of the model. The model is based off of Hui Shao's NDI design and includes the key components: a hydrophilic head and a flat, aromatic, hydrophobic body, which create an amphiphilic compound whose nature will drive the self-assembly. The hydrophobic portion will allow for π-stacking when placed in polar solution and will be forced to the inside of the structure. The hydrophilic head will have favorable interaction with polar solvents forcing it to the outside of the structure. These favorable

interactions will be the driving force for nanotube formation. Slight changes to the lysine were made based on the design changes that were done to the NDI design to try and crate different nanostructure formations. Changes made to that portion were shown to have large effects on the solubility and nanostructure formation of the NDI design.[30] It was found that with the drug model design the slight changes in the lysine induced different assemblies. Also, different solution compositions, polarity and pHs were found to have an effect on the type of nanostructure formed. A time-delay experiment showed the potential for a dynamic system to be created based on the morphologies of tumors and compound structures.

2. Synthesis of Amphiphile

The general design of the camptothecin derivative is based upon the NDI-lysine nanotube design.[24] In replacement of the chromophore in NDI, camptothecin, another mostly flat and aromatic compound, will be used to create the pi-stacking to align the compounds into "strips." The lysine end will be kept with a methyl ester to form the polar head of the compound. The same amphiphilic nature should be the same powerful driving force in creating bilayer tubes.

Compound **1.0** was created using solution synthesis to maximize yield. However, the inherent lack of solubility of camptothecin made further reactions and modifications difficult using solution based synthesis alone. Therefore both compounds **2.0** and **3.0** were made via solid-support synthesis using the appropriate resin (Wang and Trityl Resin). Instead of a base for a long polypeptide, the resin served as a solid, stable protecting group for the lysine and it allowed for easier modifications without unwanted precipitation occurring mid-reaction prior to completion. Solid support synthesis also allowed for only one purification reaction which prevented the loss of camptothecin compounds on silica-based columns after each solution reaction.

2.1 Lysine Derivative Synthesis (Compounds 1.1-1.2)

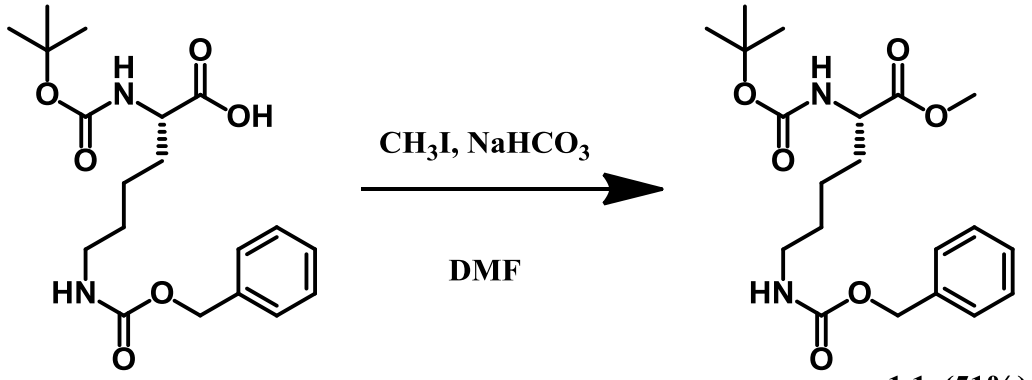

1.1 (51%)

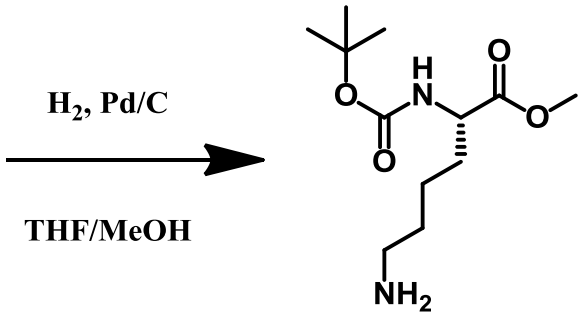

1.2 (73%)

Boc-Lys-OMe is not readily available is made through methyl esterification of the protected amino acid Boc-Lys(Z)-OH.[34] Boc-Lys(Z)-OH was dissolved in dry DMF (0.35 M), and methylated via methyl iodide and sodium bicarbonate then isolated via extraction from aqueous solution with DCM **1.1**. Deprotection of the side chain amine is done through hydrogenation Pd/C and isolated through filtration through celite, **1.2**. Both reactions form clear oils which are not crystallized prior to next steps, NMR shows purity.

2.2 Campothecin Linker Synthesis (Compound 1.3)

Camptothecin (CPT) was attached to succinic acid to create a linker by which to attach the lysine.[31]

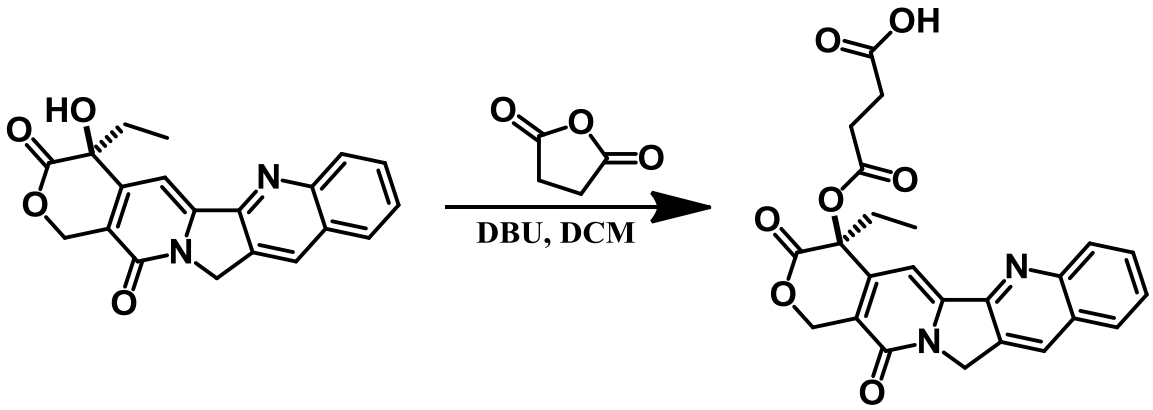

1.3 (98%)

The succinic acid is attached to the camptothecin as a linker by reacting the camptothecin with succinic anhydride and DBU. Reaction is worked up through acidification and extraction. Product is purified via trituration in MeOH **1.3**.

2.3 Methyl Ester Amphiphile Synthesis (Compounds 1.4 and 1.0)

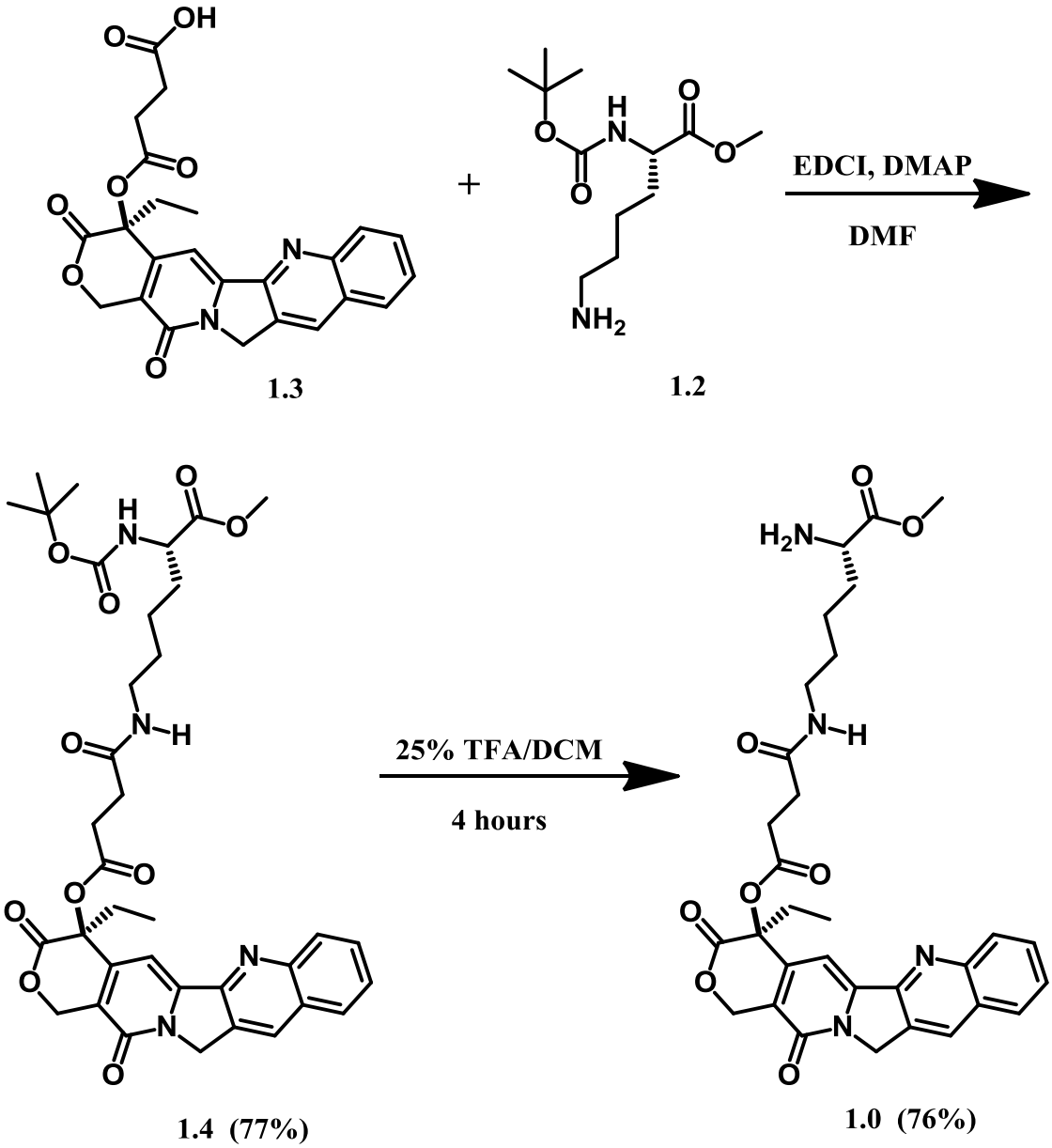

1.3 **1.2**

1.4 (77%) **1.0 (76%)**

The modified and Boc protected lysine was then attached to the camptothecin-linker via EDCI coupling with DMAP dissolved in DMF and stirring for 2 days. The solvent from the resulting solution was evaporated. The product is purified via column chromatography, **1.4**. The Boc protecting group was then be cleaved under acidic conditions. The product was then be purified by HPLC and solution with product was placed on lyopholizer to remove H_2O, **1.0**. The solid, **1.0**, was then used for studies in CD, UV, and TEM.

2.4 Free Acid Amphiphile Synthesis (Compound 2.0)

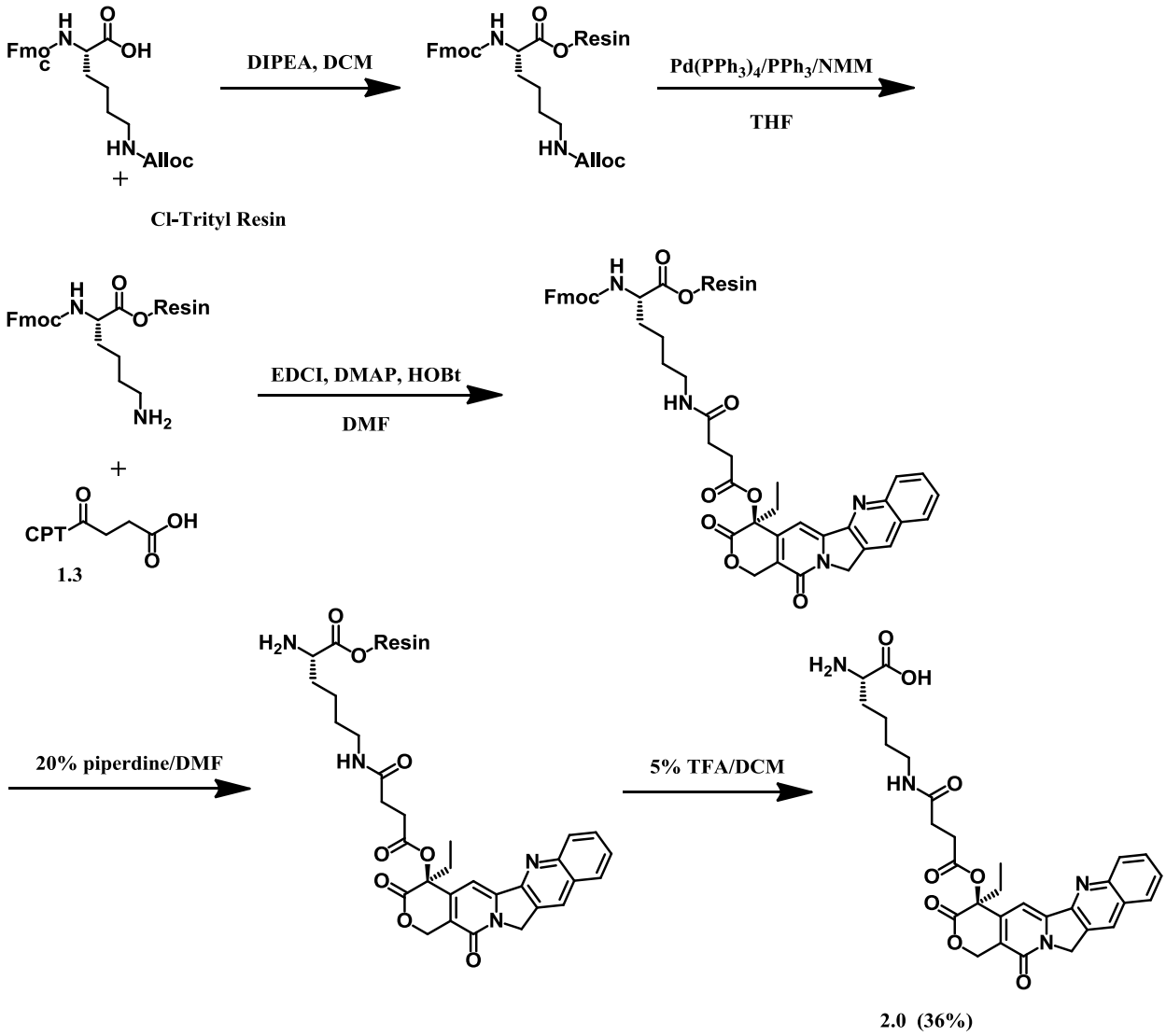

The free acid was synthesized on Trityl-Resin solid support according to standard procedures as demonstrated in the above diagram. Protected lysine was first attached to deprotected resin. The side chain protecting group was cleaved and the camptothecin linker was attached. The amino group was then deprotected and the compound was cleaved from the resin. The product was precipitated after the solvent was removed and purified by HPLC.

2.5 Amide Amphiphile Synthesis (Compound 3.0)

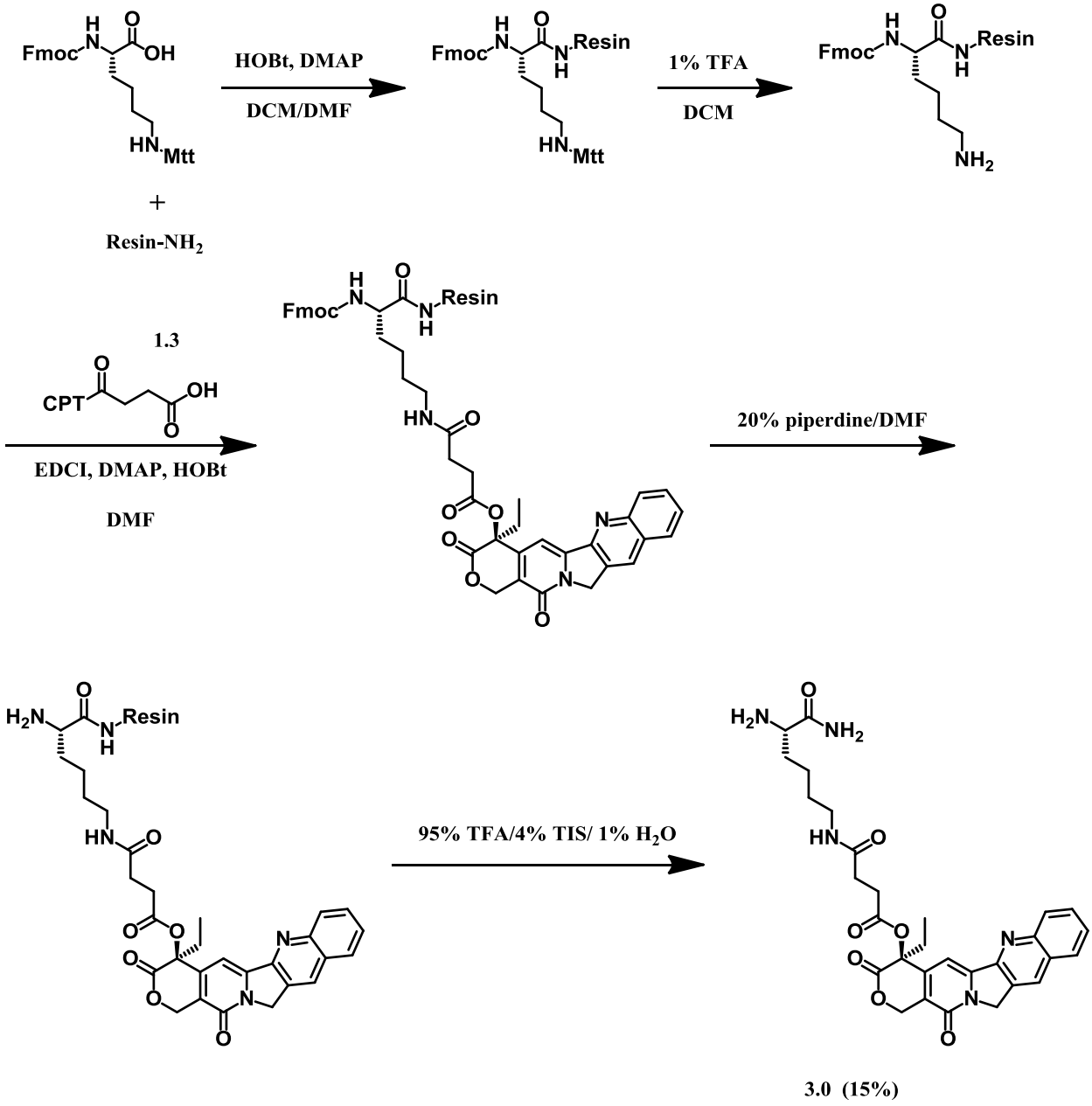

The amide was synthesized on Rink-Resin solid support according to standard procedures as demonstrated in the above diagram. Protected lysine was first attached to deprotected resin. The side chain protecting group was cleaved and the camptothecin liker was attached. The amino group was then deprotected and the compound was cleaved from the resin. The product was precipitated after solvent was removed and purified by HPLC.

2.6 Compound Description and Solubility

Campothecin in its natural form is not soluble in the majority of solvents, including water which is a requirement for intravenous injection, the method by which chemotherapeutic agents are typically delivered. To make a viable drug, ideal solubility for testing is in phosphate buffer solution (PBS) as a mimic to physiological condition.

Compound **1.0**: a yellow, fluffy solid, similar in color to natural camptothecin. Solubility in water, PBS, and organic solvent (TFE) was determined by creating 10 mM solutions. The compound was placed in appropriate amount of solvent and then sonicated with mild heating to induce complete solvation. Despite its inherent lack of solubility, the final compound was readily soluble in TFE, forming a bright yellow solution. The final compound was also soluble in both H_2O and PBS at 10 mM concentration after slight agitation via sonication and slight application of heat.

Compound **2.0**: a yellow, fluffy solid, similar in color to natural camptothecin. Solubility in PBS after agitation via sonication and mild heating was determined for 5.7 mM solutions with turbid appearance. Not soluble in neutral water.

Compound **3.0**: orange/yellow, fluffy solid, darker in color than natural camptothecin. Compound was not soluble in neutral aqueous solution. Compound was soluble in PBS . Solution had slightly turbid appearance and required sonication for complete solvation.

3. Results/Discussion

3.1 UV and CD Characterization

3.1a Methyl Ester Amphiphile

Samples of compound **1.0** were prepared in each H_2O, PBS and TFE solutions at 10 mM and aged 2-4 days. Solutions were then diluted to specified concentration just prior to testing.

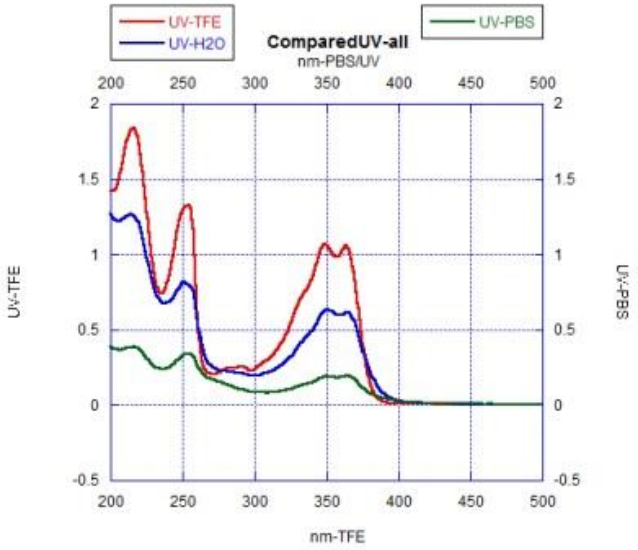

Figure 3.1 Comparison of UV scans of 3 dilutions of Compound 1.0 at 0.5 mM concentrations

The UV patterns of all three solutions are similar in the peak wavelengths. Absorbance occur at 210 nm, 250 nm, 350 nm and 360 nm for each of the solutions. The peaks in the TFE solution have higher relative absorptions than either the H_2O or PBS solutions. However, there is also a distinct difference in the relative absorptions of the H_2O and the PBS solutions. The more defined aggregates of the H_2O (nanotubes) result in a higher absorbance in the UV than the random aggregates that formed in the PBS solutions. Comparing this result with the TFE which also formed defined aggregates, fiber structures, the more defined aggregates result in higher UV absorbance than the less defined aggregates. These peaks also align closely with the peaks or directly between two peaks that occur in each of the CD patterns.

a)

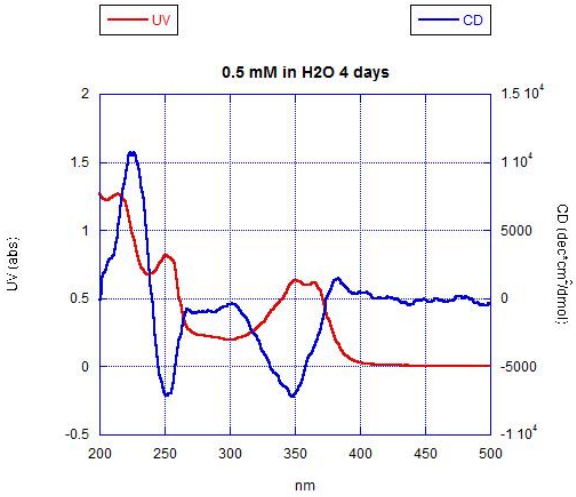

b)

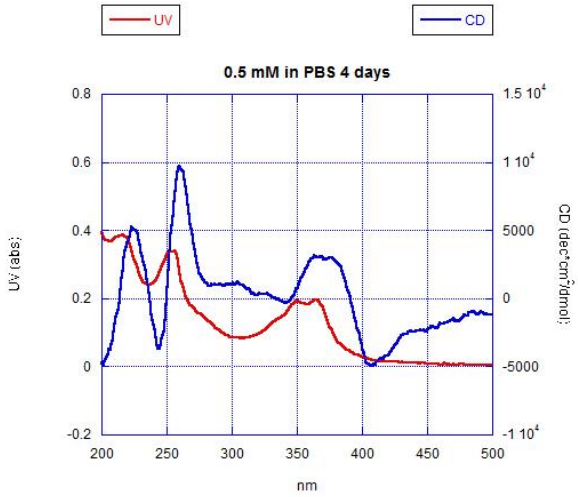

c)

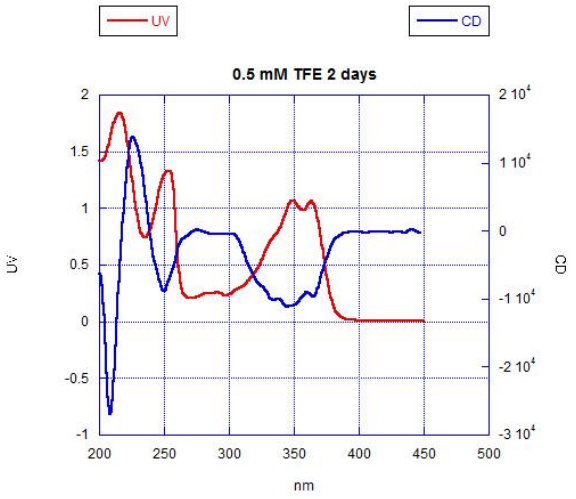

d)

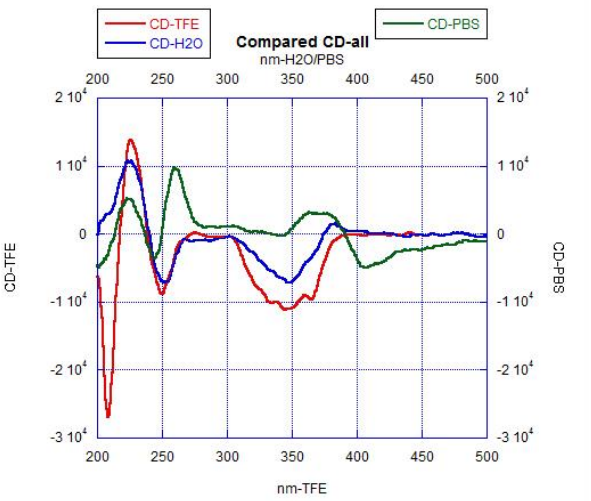

Figure 3.2 a) CD and UV of 0.5 mM solution in H_2O after 4 days of aging at 10 mM b) CD and UV of 0.5 mM solution in PBS after 4 days of aging at 10 mM c) CD of 0.5 mM solution in TFE after 2 days of aging at 10 mM d) Comparison CD of all 3 diluted solutions of 0.5 mM concentration (all CD measurements are in deg*$cm^2$$dmol^{-1}$)

Each of the circular dichroism (CD) scans display peaks near 350 nm and between 200 and 250 nm which correlate to the absorptions seen in the UV patterns. . The UV absorptions of the three solutions all fall either at a peak or at the midpoint between two peaks. This result indicates that the UV absorptions are coordinated to the same stacking or aggregation patterns as indicated by the CD. Peak patterns in the UV spectra indicate the creation of chirality beyond the

camptothecin chiral centers suggesting stacking of the compound occurred π–π interactions. At first glance, all three CD patterns show similarities in their peak locations. However, placing all three sets of data on the same graph (fig 3.1d) shows very clear distinctions between the three patterns. All three solutions have a peak at 225 nm and then an inverse peak when at 250 nm But the three solutions display unique patterns between 300 and 400 nm that differentiate them. The TFE solution appears to be an exaggeration of the H_2O solution. But, the compound dissolved in PBS shows a distinct pattern that does not mimic either of the other two. The three unique patters displayed in CD indicate that it is very likely that three different nanostructures will emerge when observing the solutions with a TEM, as unique patterns reflect unique structure formations.[32] However, none of the patterns line up with patterns CD patterns observed with the NDI based nanotubes.[13, 26, 32-33]

3.1b Free Acid and Amide Amphiphiles

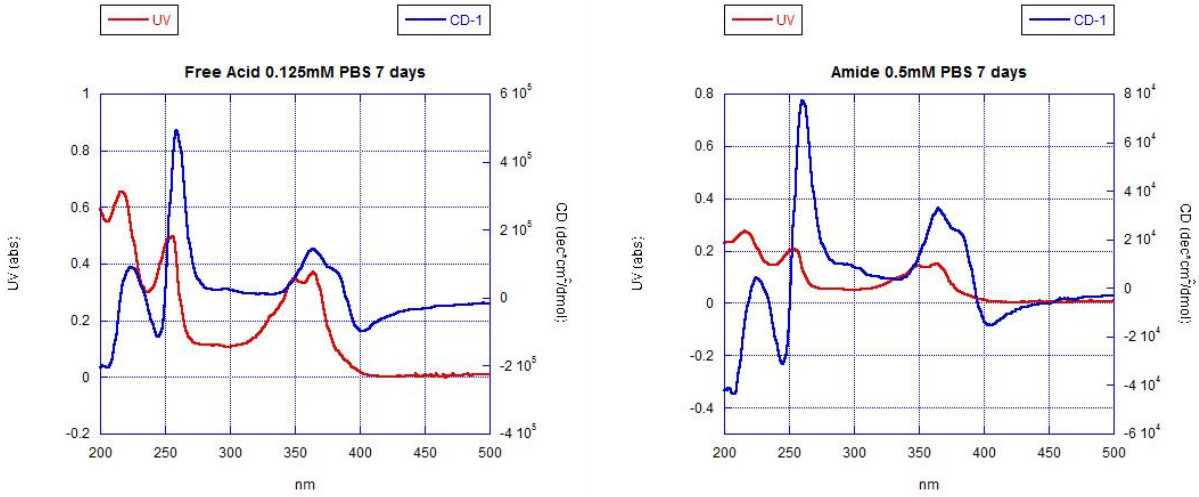

Figure 3.3 UV and CD of Free Acid (**2.0**) and Amide Amphiphiles (**3.0**) in PBS. (all CD measurements are in deg*$cm^2$$dmol^{-1}$)

The CD and UV scans were performed on the compounds **2.0** and **3.0** after 7 days of aging in 8.7 mM and 5.3 mM solutions respectively. Both solutions were then diluted to 0.125 mM and 0.5 mM respectively for testing. Both amphiphiles show similar peak patterns between

350 and 400 nm as well as cotton effects at 250-265 nm and a final peak 225 nm. After normalization, the free acid amphiphile (**2.0**) shows higher peaks in the CD scans than the Amide (**3.0**) by a factor of 10. The UV absorptions are also stronger but not to the same scale. These similarities indicate that a similar pattern of stacking and nanostructure formation has occurred. This hypothesis was later confirmed by the formation of similarly sized nanotubes visualized by TEM.

3.1c Comparison of 3 Designs

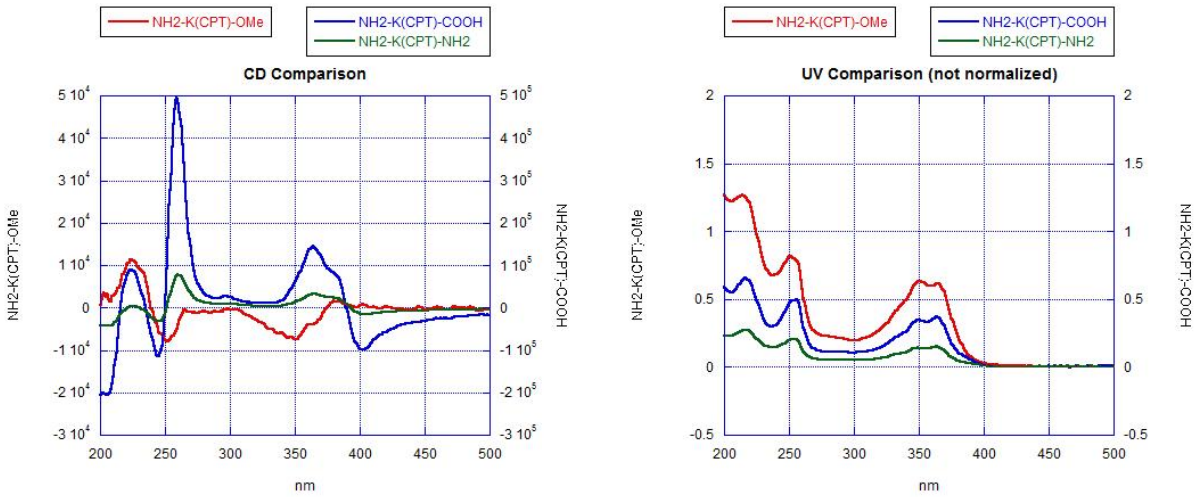

Figure 3.4 UV and CD of 3 Designs in H_2O and PBS. (all CD measurements are in deg*cm^{2}dmol^{-1})

Comparing the CD and UV patterns can shed light on similarities that may exist in the amphiphile stacking and nanostructure formation. The methyl ester design (**1.0**) was scaled to increase the relative peak heights for accurate comparison. As stated above, compounds **2.0** and **3.0** designs show similar CD excitation patterns but differ by a factor of approximately 10 in strength. This similarity indicates that the two will follow a same stacking pattern. Compound **1.0** has a dramatically different peak pattern in water where it formed nanotubes in comparison with the other two patterns as well as over 100 fold difference in strength of peaks. The near inverse excitation pattern between 350 nm and 400 nm suggests that the camptothecin is stacking

differently perhaps with an oppositely styled twist. Though while a different pattern emerges, the excitations occur at similar wavelengths indicating that camptothecin and lysine stacking is still occurring just in a different manner. The TEM images confirm a different nanostructure in terms of wall width but indicate no difference in overall formation (sheet-stacking theory explained below).

The UV patterns show similar absorbencies at the same wavelengths that excitations in the CD were observed. The differences in overall absorbance are explained by the difference in the concentration of the samples when testing occurred. Both the amide and the methyl ester were observed in 0.5 mM concentrations which allow comparison. The absorption is significantly decreased in the amide solution in comparison to methyl ester and is smaller than the free acid absorptions which were taken a smaller concentration (0.125 mM).

3.2 TEM Characterization

Sample dissolved in 10-13 mM solutions in water, PBS or organic solvent. Samples then prepared for TEM[12]: 10 μL drops of sample solution were applied to carbon-coated copper grid (Ted Pella, Inc.) for 2 min and after removal the excess solution with filter paper, the grid was floated on 10 μL drops of 2 wt% uranyl acetate solution for negative stain for 2 min. The excess solution was removed by filter paper. The dried specimen was observed with Technai G2 Spirit instrument operating at 80 keV. The data were analyzed with Image pro software.

3.2a. Methyl Ester

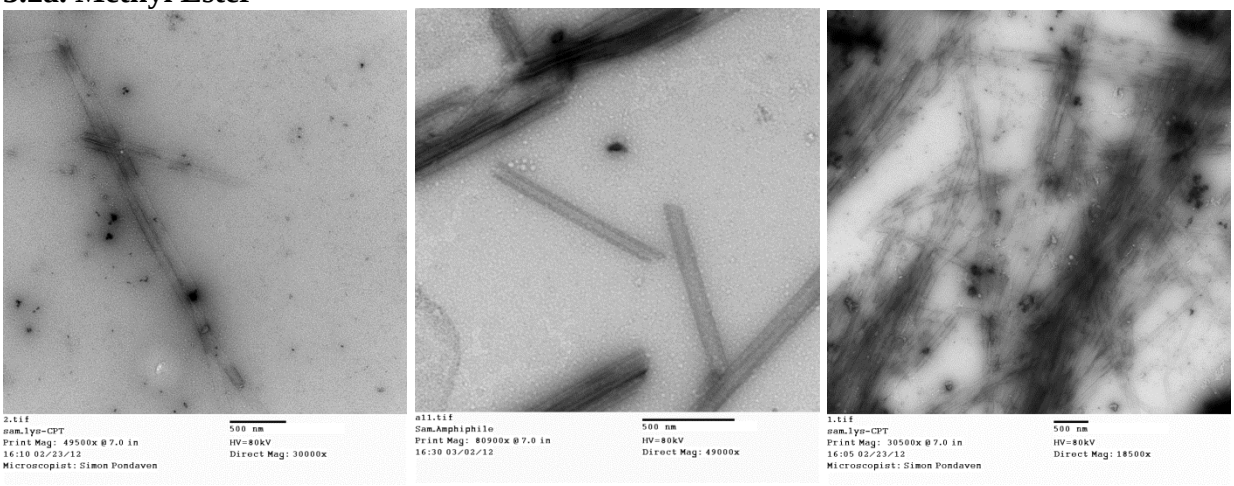

Figure 3.5 Nanotubes formed in 10 mM solution of H_2O and diluted to 0.5 mM for imaging. a) Two sets of paired nanotubes crossing after 4 days. b) Individual nanotubes with distinct walls after 7 days. c) Cluster of nanotubes after 7 days *(all scale bars measure 500 nm)*

After four days of aging in 10 mM solution and another three days of aging at 0.5 mM concentration, TEM images were taken of the aqueous solution. The images indicate the formation of nanotubes. The nanotubes were generally seen in clusters as in Fig. 3.5c, where individual nanotubes were difficult to distinguish from one another. Isolated nanotubes were observed and characterized, as in Figs. 3.5a and 3.5b. The nanotubes were found to have a total diameter of 95 nm, within the 10-100 nm limit for the EPR effect, and wall widths of 20 nm. The approximate length of a single nanotube was measured to be 2 nm. The wall thickness and wide

hole through the middle of the tube indicate a sheet stacking and then rolling theory. The compound stacks with the hydrophobic portions lining up head to head and stacking next to each other forming sheets.

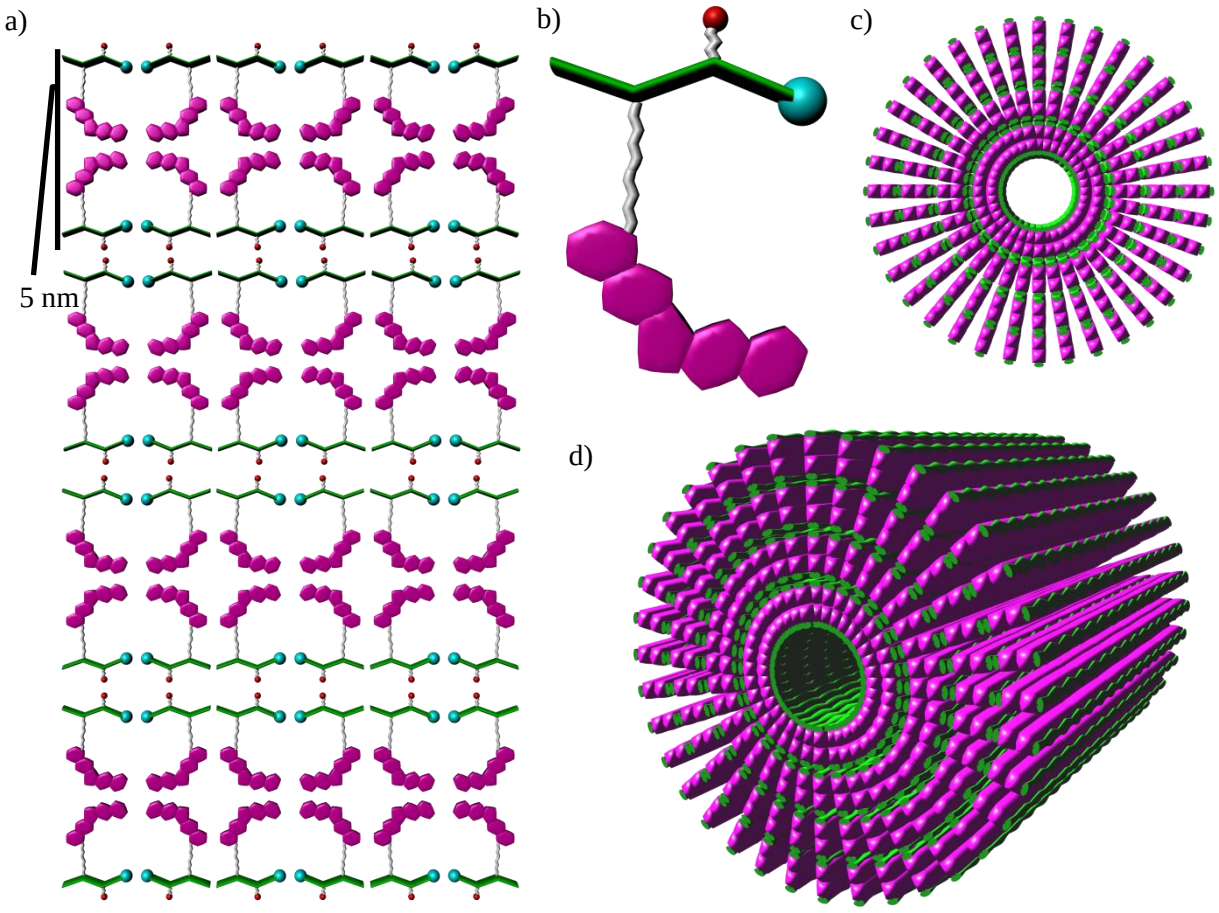

Figure 3.6 Sheet Stacking Theory, multiple sheets (2+) stack and roll to form tube. a) view of 4 stacked bi-layers of amphiphile sheet. b) single amphiphile (2 nm). c) view of nanotube from side. d) view of nanotube at angle

These sheets are formed on top of one another and proceed to roll into a tube. A similar stacking has been observed with tetra-peptide models formed by other lab members as well as structures proposed for the NDI-peptide compound that formed nanotubes.[26] TEM images determine the wall thickness to be 20 nm which suggests the stacking of 4 sheets together, as each sheet measures 5 nm, which then proceed to roll. This stacking theory allows for the

hydrophobic portions to be maintained together and protected from the aqueous solution. It is the hydrophobic stacking that is the driving force for the nanotube formation.[26] The measurements for tube diameter and wall thickness are consistent throughout the images taken. Thus, a stabilized and defined structure has been made that encapsulate the drug; though, there is slight variation on the length of each tube, all near 1 micron, some larger and some smaller. None shorter than 500 nm was isolated. The isolated tube has a length of slightly more than 1 micron (Fig. 3.3b), but definitive measurements of other images are difficult to obtain with the clustering of the nanotubes. The clustering obscures the ends of the tubes. The aqueous assembly in all other aspects meets the ideal aspects for drug delivery systems.[11]

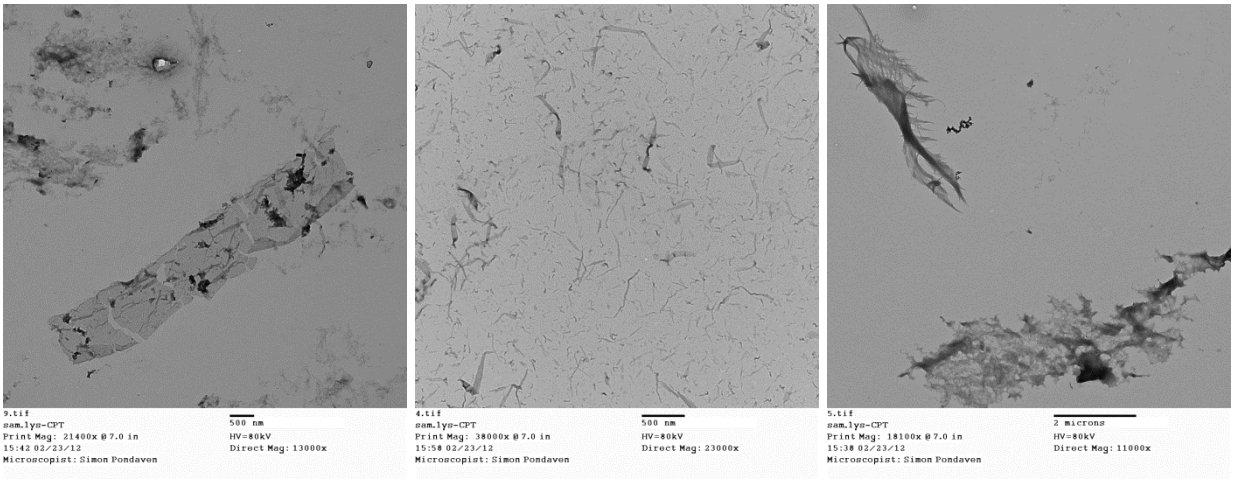

Figure 3.7. Nanostructures formed in 10 mM PBS solution, aged 4 days, diluted to 0.5 mM for imaging. a) Partial β-sheet formation, surrounding by random aggregates. b) Small fibril structures. c) Random aggregate formation *(a and b scale bars measure 500 nm, c measures 2 microns)*

After 4 days of aging at 10 mM concentration and then 2 days at 0.5 mM concentration, the above images were taken via TEM. It can be observed that unlike in water, no stable aggregates form in PBS. A variety of structures appeared including disrupted β-sheet formation, random fibers and, for the majority of the grid, random aggregates as in Fig. 3.7c were observed. While, the CD scans indicate that stacking had occurred of the lysine and the camptothecin, the

stacking appears disordered and unstable. The disarray observed in the PBS images is most likely due to salt inference of the stacking of the different portions of the compound. Interactions of the hydrophilic portions of the compound and the salts would disrupt stacking effects seen in the water solutions. The camptothecin is not a completely planar structure, as was the NDI structure used in the semiconductor model. Thus, its stacking ability is decreased from the onset. Without the aid of the hydrophilic portions, it appears the hydrophobicity of the camptothecin is not enough to force stacking, β-sheet, and tubular formation.

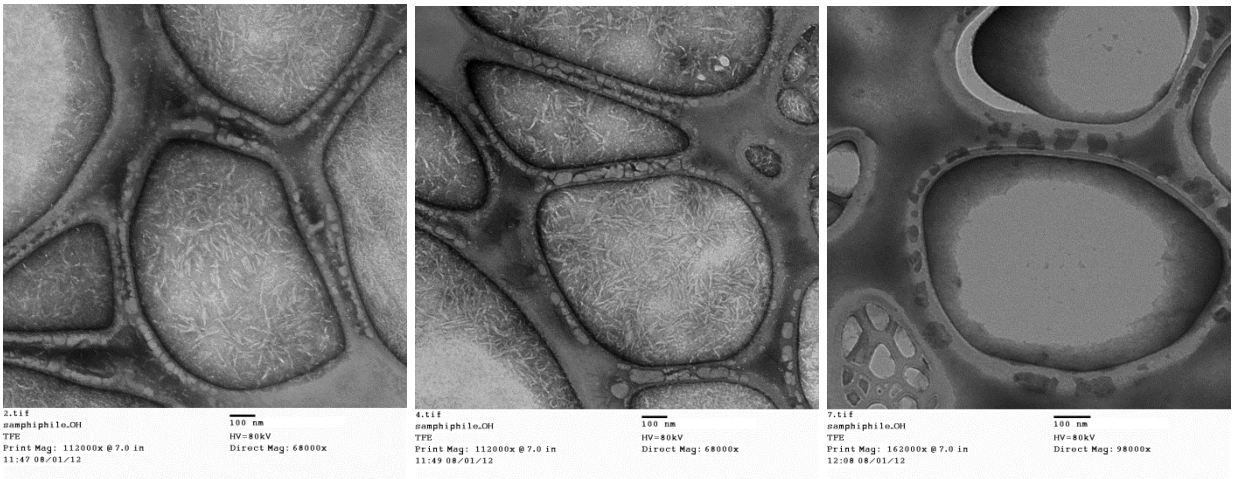

Figure 3.8. TEM images of TFE solutions displaying fibers a) & b) 10 mM solution after 5 days aging, random fibers. c) No nanostructures in 10 mM solution diluted to 0.5 mM solution for imaging. *(all scale bars measure 500 nm)*

The compound was readily soluble in TFE solution and did not require agitation or heating to obtain complete solubility at 10 mM. After 5 days of aging, images were taken of the 10 mM solution. Images of large clusters of nanofibers were observed (Figs. 3.8a and 3.8b). However, the diluted solution, 0.5 mM, showed no nanostructure formation (Fig. 3.8c) despite excitations in the CD spectra observed at that concentration after 2 days of aging. Low concentrations may not have close enough interactions of the compound to yield visible nanostructures via TEM despite the CD results. However, as structures are observed at higher concentrations, it can be said that self-assembly occurs in TFE.

All three solutions yielded differing CD excitation patterns and different nanostructures in TEM imaging, as would be expected. The UV absorptions occurred at the same wavelengths for all three solutions and aligned with the CD excitations.

3.2b Free Acid Amphiphile

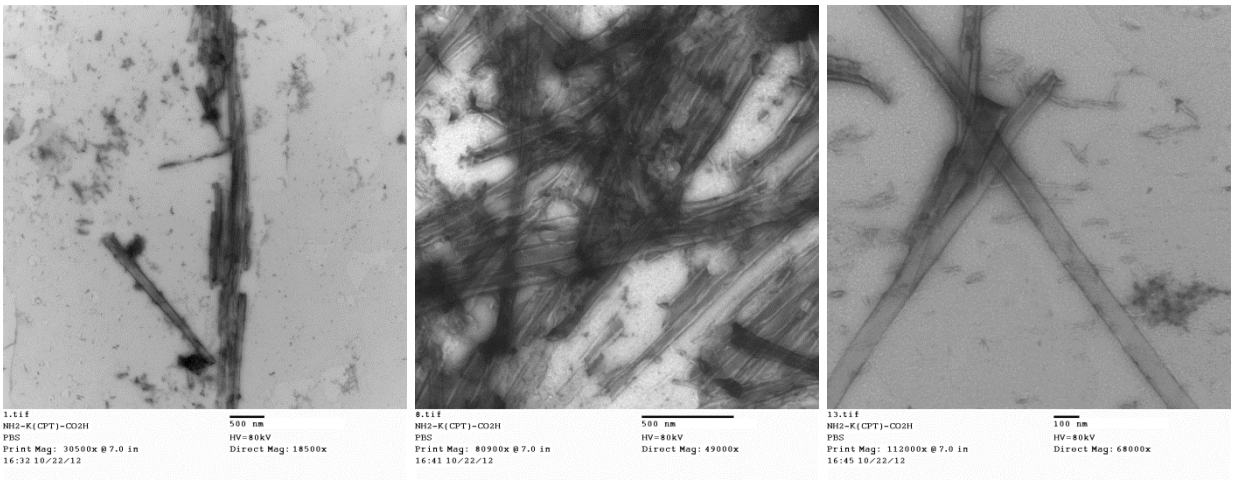

Figure 3.9. TEM images of compound in 5.7 mM solution after three days of aging in PBS. Scale bars a) and b) measure 500nm, c) measures 100nm.

Compound 2.0 was not readily soluble in PBS; solution was slightly heated and then sonicated for an hour to aid in solubility. Compound was aged for three days, prepared and then imaged with via TEM. Images indicate the formation of nanotubes. The nanotubes are between 80-175 nm in diameter with the majority of tubes having a diameter between 80-100 nm, Fig. 3.9c shows a consistent diameter of 92 nm for the right nanotube. The nanotubes have a wall thickness of 16 nm. This size indicates a similar formation pattern to the tubes imaged of the methyl ester amphiphile in water, 3 layers. The smaller wall thickness would indicate the stacking of three sheets as opposed to four due to the width of a bilayer being 5 nm.

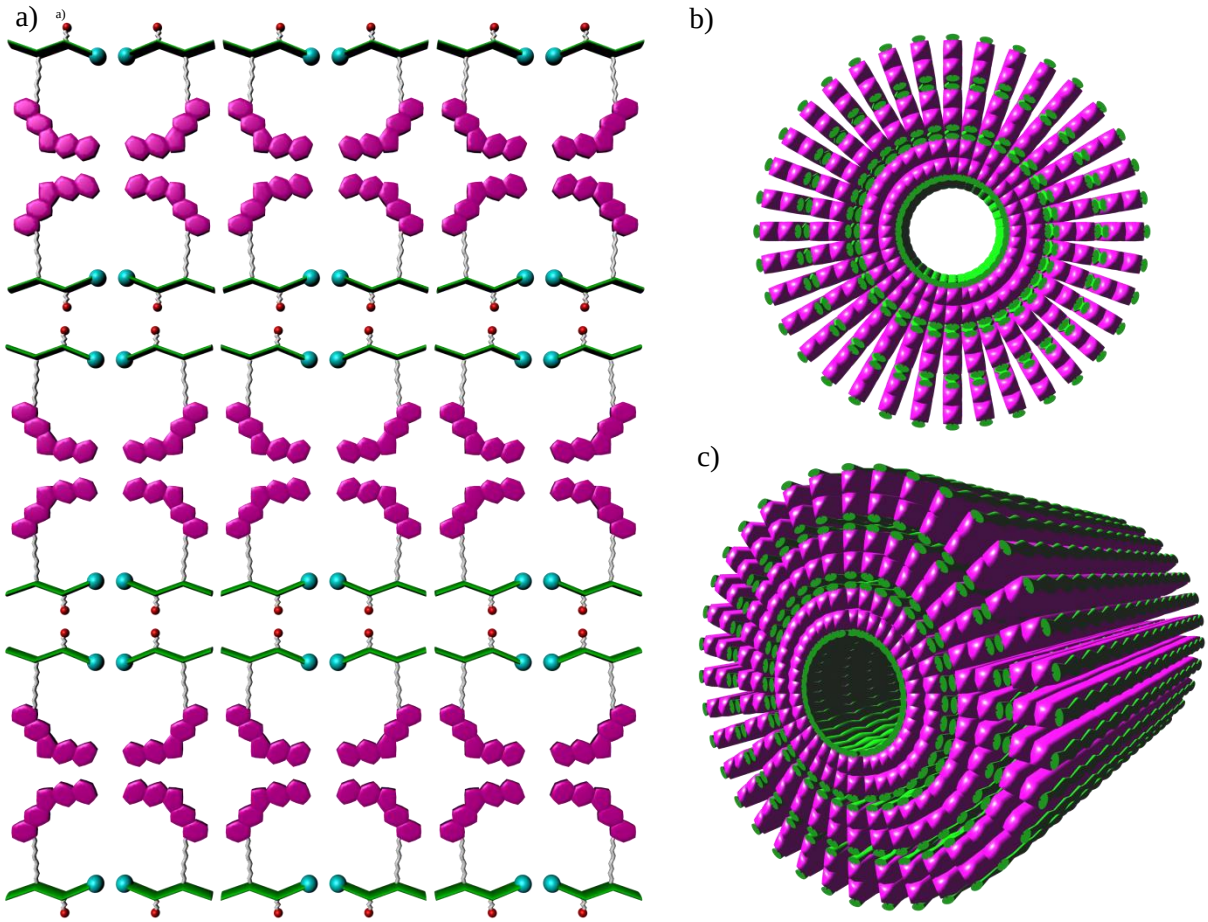

Figure 3.10. Sheet Stacking Theory, multiple sheets (2+) stack and roll to form tube. a) view of 3 stacked bi-layers of amphiphile sheet. b) view of nanotube from side. c) view of nanotube at angle

As opposed to the methyl ester, the PBS solution aided in the solubility in comparison with water and produced stabilized aggregates. The increased salt concentration of the solution, and thus anionic species concentration, increased the stacking and formation of tubes. This anionic effect has been seen with other nanostructures to be affecting the formation and can have a drastic effect.[34] The salts in solution interact favorably with the zwitterion and aromatic regions, as opposed to unfavorably as seen with the methyl ester amphiphile, to make tube formation thermodynamically favorable.

3.2c Amide Amphiphile

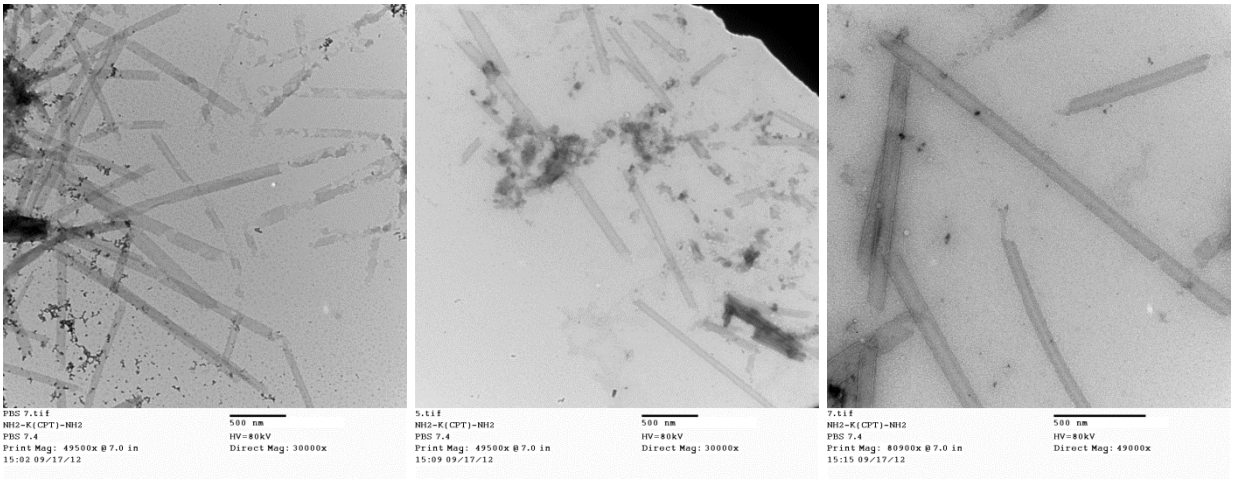

Figure 3.11. TEM images of amide amphiphile after three days aging in PBS. a) broken nanotubes/formation of nanotubes. b) and c) full and stable nanotube. Scale bars 500 nm.

Compound required sonication in order to become fully soluble at high concentrations in PBS. After 3 days aging, TEM images were taken of concentrated samples which show nanotube formation. Nanofiber formation was not seen in images of the amide amphiphile in PBS in contrast with the Free Acid amphiphile which displayed fibril and nanotube formation after the same aging time. Nanotubes formed in PBS solution do not all form as the same diameter and wall width in contrast with the other two compounds which display equal diameter and wall width across all nanotubes imaged. The nanotubes formed from the amide amphiphile show a range of dimensions: 70-95 nm in diameter and 18-26 nm in wall width. A larger diameter size did not always coordinate with a thicker wall width. The size of the tubes and wall widths indicate a similar assembly process as other two compounds, specifically compound **2.0** due to similarities in the CD scans but with 3-5 β-sheet stacks.

***Study done with PhD. candidate Se Hye Kim

3.3 Time Delay Experiment- Dynamic System Test

Solution of Compound 1.0 was prepared at 10 mM concentration in H_2O and aged for 4 days. Solution was then diluted to 1.0 mM in H_2O for baseline UV and CD. Concentrated H_2O solution was then diluted to 1.0 mM solution using PBS. CD was used to determine if change in nanostructure, after having been formed in one type of solution, occurs when solution composition has been changed.

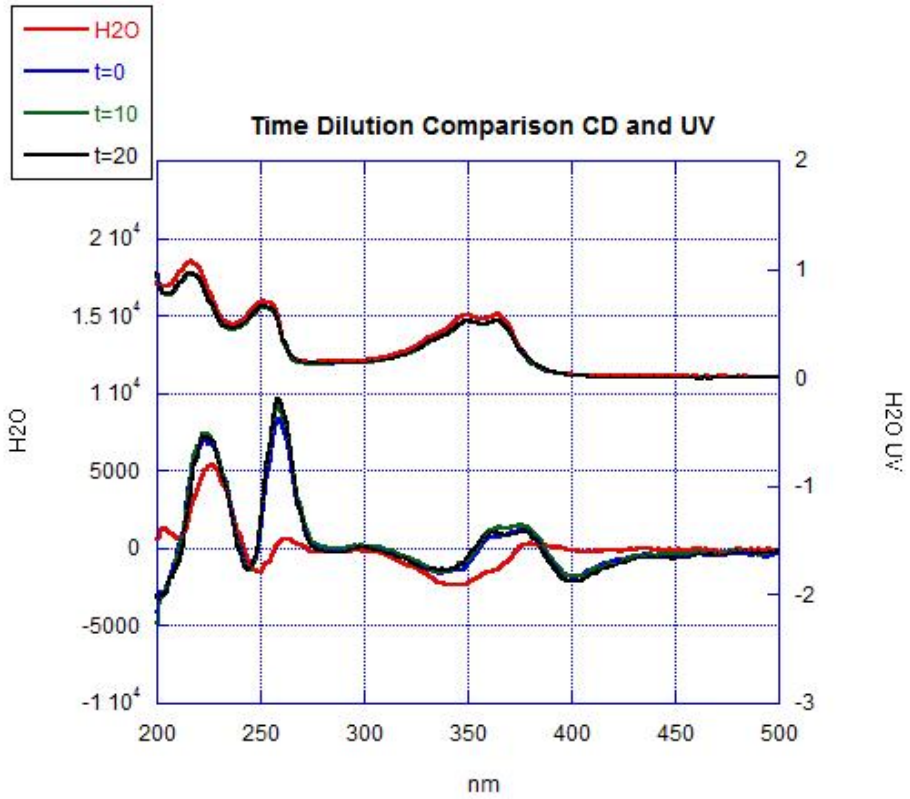

Figure 3.12 Dynamic System Test CD and UV comparison. t= time CD scan was initiated starting at 800 nm, ~ 3 minutes to 350 nm

The two CD forms show unique excitations patterns that can be distinguished from another, indicating the two different nanostructure formations. The initial dilution in water demonstrates the same peak pattern as observed in the previous experiments from which the nanotubes were imaged. The CD scan takes approximately 3 minutes to go from 800 nm to the 350 nm range where clear differences in the spectrum may be observed. The times represented in

the graph are time after solution was diluted at the beginning of the scan (800 nm). The first scan taken of the dilution (t=0) in PBS, shows a change in pattern from H_2O to a pattern matching the previously taken PBS patterns. All measurements taken after the PBS dilution show the PBS solution excitation pattern. This data indicates that there was a change from the nanotube structure that the H_2O pattern indicates to the random aggregate structure that formed in PBS solutions. This result occurred despite the aging in water and dilution in PBS. Therefore, the compound is able to have a complete confirmation and stacking change immediately (within 3 minutes) of having an environmental shift. The UV patterns of all three solutions match each other as well as match the original UV patterns taken from the samples that were imaged. There is a slight depression in strength going from the H_2O dilution to all of the PBS dilutions. This result matches the depressions that occur when each of the solutions were aged and diluted via the same medium.

4. Conclusion

The three models designed and tested showed slightly different assemblies and had varying solubilities in water and PBS (soluble in 10mM or greater solutions was defined as soluble). All three formed nanotubes but of the three only the compound 2.0 and the 3.0 showed both solubility and nanotube formation in PBS, solution used as a mimic for human blood conditions for purposes of testing and imaging. The amphiphilic nature of the designs causes their assembly into nanotubes, driven by hydrophobicity. The increase in polarity at the hydrophilic head decreased the solubility of the last two designs leading to their limited solubility, soluble in PBS but not neutral water. The ions in the PBS solution interacted with the compound 1.0 in an unfavorable manner leading to the formation of random aggregates as opposed to stabilized nanostructures as was seen in water. However, due to the anionic effect where the ions in the PBS solution interact with the hydrophilic head group, the opposite was demonstrated by the compound 2.0 and 3.0 designs. Both showed an increase in stacking (as seen in CD excitation strength increases) and formed stabilized nanotube structures that demonstrate similar formations. The increase in the polarity of the solution could also cause increased camptothecin stacking in the last two designs as well, leading to an increase in CD excitation signal and could lead increased stabilization.

It was shown that a dynamic system is possible but further modifications need to be made; such as increasing the polarity of the head, decreasing the length of the linker, or changing the number of amino acids used as the polar portion (making a di- or tetrapeptide) that are sensitive to slight change in acidic conditions that would occur in tumor cell environments.

Possible modifications to the design, such as changing the linker length or drug type, could lead to a smaller and more stable nanotube. This change would allow for the EPR effect to

be taken advantage of even more. Also, the shorter linker would cause a more rigid structure potentially increasing its sensitivity to slight environment changes.

The designs that show nanotube formation in PBS (human blood mimic) will be tested for their efficacy and toxicity in mice models of pancreatic carcinoma in the lab of Dr. Mark Grinstaff at Boston University.

5. Experimental

General Methods. All reagents were used as received unless otherwise noted. All solvents used in reactions were distilled using appropriate measures prior to use. Dimethylformamide was dried and stored over 4 Å molecular sieves. All reactions were performed under nitrogen unless otherwise indicated and monitored by TLC with spots detected under UV light. Circular dichroism (CD) spectra were taken on a AVIV 202 CD Spectrometer. Transmission Electron Microscopy (TEM) was performed on a Technai G2 Spirit instrument operating at 80 kV. ^{1}H NMR were recorded at 250 or 400 MHz and ^{13}C NMR were recoreded at 400 MHz on a Bruker DPX-250 or DPX-400 instrument as noted. Chromatographic seperations were done on silica gel 60 (230-400 mesh, 60 Å) using the noted solvents. All water used for solutions was HPLC grade.

Peptide Resin Synthesis.

Resin based synthesis was done using either Rink Amide Resin (0.59 mmol/g) or Trityl Resin(1.00 mmol/g). Attachment of lysine to rink amide resin was performed by Fmoc-Lys(Mtt)-OH, 1,3-diisopropylcarbodiimide (DIC), and 1-hydroxybenzotriazole (HOBt) (300 mol% each relative to resin) in 1:1 DMF:DCM for 2 h. Trifluoroacetic acid (1%) in DCM was used for Mtt deprotection. Attachment of lysine to Trityl Resin was performed by Fmoc-Lys(Alloc)-OH (200 mol%) , N,N-Diisopropylethylamine (DIPEA) (400 mol%) in DCM for 24 h. Alloc was deprotected by $Pd(PPh_2)_4$ (50 mol%), N-methyl-aniline (450 mol%), and PPh_3 (450 mol%). CPT-linker was then attached via (300 mol% each) 4-Dimethylaminopyridine (DMAP), 1-ethyl-3-(3-dimethylaminopropyl) carbodiimide (EDCI) and 1-hydroxybenzotriazole (HOBt) in DMF for 48 h. Piperdine (20%) in DMF was used for Fmoc removal. The CPT-peptide was cleaved from the resin by treatment with TFA/water/triethylsilane (95/2.5/2.5) for the Rank-resin and 5%

TFA/DCM for the Trityl Resin at room temperature for 2 h. Crude products were precipitated with cold ethyl ether and purified by reversed-phased HPLC on preperative Varian Dynamax C18 column and stored as lyopholized powders at 0°C.

Circular Dichrosim (CD) Spectroscopy Measurement.

CD spectra were recorded on an AVIV 202 CD spectrometer under a nitrogen atmosphere. Experiments were performed in a quartz cell with a1 mm path length over the range of 190-800 nm at 25 °C.

Electron Microscopy Measurement- Negative Stain TEM.

10 μL drops of dilute amphiphile (5-10μL) were applied to carbon-coated copper grid (Ted Pella, Inc.) for 2 min and. After removal the excess solution with filter paper, the grid was floated on 10 μL drops of 2 % wt uranyl acetate solution for negative stain for 2 min. The excess solution was removed by filter paper. The dried specimen was observed with Technai G2 Spirit instrument operating at 80 keV. The data were analyzed with Image pro software.

Mass Spectrometry ESI.

Samples were dissolved in either water, MeOH or CH_3CN and spectra was recorded on Bruker MicrOTOF (ESI).

Synthesis of Compound 1.1[35]

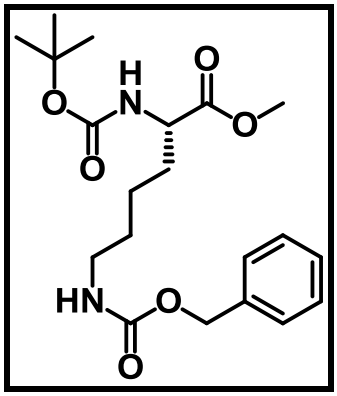

In a 10 mL round bottom flask, Boc-Lys(Z)-OH (0.500g, 1.314 mmol) and $NaHCO_3$ (0.331 g, 3.942) were dissolved in DMF (4 mL). To the reaction CH_3I (0.210 g, 1.446 mmol, 0.09 mL) was added in one portion. The reaction was stirred for 17 h and then diluted with EtOAc (20 mL). Organic solution was washed with H_2O (2 x 15 mL) and brine (10 mL). The organic layer was dried with anhydrous sodium sulfate, filtered and organic solvent was removed in vacuo. Product was purified via column chromatography (10:1 CH_2Cl_2:MeOH, R_f**:** 0.6) yielding clear oil (0.378 g, 73%). ^{1}H NMR (250 MHz, DMSO) δ 1.32-1.37 (m, 11H), 1.55-1.58 (m, 2H), 2.96 (q, 2H, J= 5 Hz), 3.60 (s, 3H), 3.85-3.94 (q, 1H, J= 7.5 Hz), 5.00 (s, 2 H), 7.20-7.23 (m, 2H); 7.31-7.37 (m, 4H); ^{13}C NMR (400 MHz, DMSO) δ 14.03. 20.71, 22.72, 27.89, 28.12, 28.85, 30.25, 35.77, 51.63, 53.47, 59.74, 65.07, 78.19, 127.64, 127.70, 128.31, 137.21, 155.56, 156.09, 173.17; ESI-MS calculated for $C_{20}H_{30}N_2O_6$ [M+Na] calc= 417.1996, obs= 417.1986; IR (DMSO) υ 3348, 3217, 3040, 1597, 1728, 1674 cm^{-1}.

Synthesis of Compound 1.2[36]

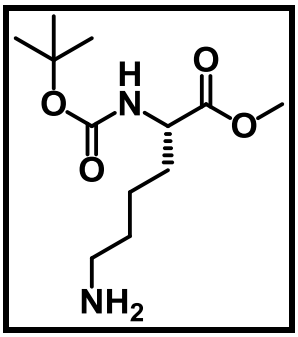

In a 10 mL round bottom flask, Boc-Lys(Z)-OMe (0.378 g, 0.9583) was dissolved in 4 mL THF:MeOH (1:1). To the solution, 10% Pd/C (1 g) was added and the reaction was placed under H_2 balloon. After 20 h stirring under H_2, the reaction was filtered through a pad of celite, washed with MeOH (10 mL). The organic solvent was removed in vacuo yielding clear oil (0.057 g, 51%). ^{1}H NMR (250 MHz, DMSO) δ 1.32-1.37 (m, 11H), 1.52-1.57 (m, 2H), 2.58-2.63 (m, 2H), 3.6 (s, 3H), 3.85-3.94 (m, 1H), 7.25 (m, 1-2H), NMR peaks consistent with literature; ^{13}CMR (400 MHz, DMSO) δ 14.05, 20.73, 27.56, 28.13, 28.81, 51.53, 52.56, 59.71, 77.91, 78.12, 128.17, 174.30; ESI-MS calculated for $C_{12}H_{35}N_2O_4$ [M+H] calc= 261.1809 obs= 261.1799; IR (DMSO) υ 3410, 3233, 1705, 1674, 1528 cm^{-1}.

Synthesis of Compound 1.3

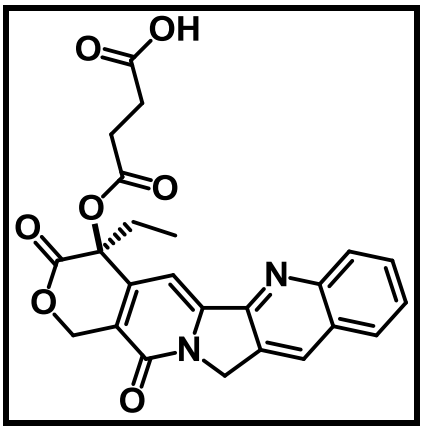

To a 25 mL round bottom flask with stir bar was added CH_2Cl_2 (13.1 mL). Camptothecin (0.150 g, 0.431 mmol) and succinic anhydride (0.129 g, 1.292 mmol) were added together and partially dissolved in solution. The solution was stirred and the reaction was cooled to 0˚C. The solution was cooled to 0°C, and DBU (0.196 g, 1.29 mmol, 0.193 mL) drop wise for 5 min and solution was stirred for 2 h. The reaction was monitored by TLC (10:1 CH_2Cl_2:MeOH) for disappearance of camptothecin. Upon completion, the reaction was washed with 5% HCl aqueous solution (20 mL) and product extracted with 10% MeOH in $CHCl_3$ (3x, 50 mL). Organic layer was dried with anhydrous Na_2SO_4. Crude was triturated with MeOH to yield yellow solid (0.190 g, 0.424, 98%, m.p. (MeOH): 205-208°C). ^{1}H NMR (250 MHz, DMSO) δ 0.90 (t, 3H, J = 5.0 Hz), 2.15 (m, 2H), 2.50 (m, 2H), 2.74 (m, 2H), 5.30 (s, 2H), 5.48 (s, 2H), 7.13 (s, 1H), 7.72 (t, 3H, J = 7.5 Hz), 7.87 (t, 1H, J= 7.5 Hz), 8.16 (t, 2H), 8.70 (s, 1H), 12.26 (s, 1H); ^{13}C NMR (400 MHz, DMSO) δ 7.49, 28.35, 28.52, 30.35, 50.17, 66.26, 75.83, 95.09, 118.18, 127.93, 127.72, 128.51, 128.99, 129.77, 130.36, 131.52, 145.21, 145.89, 152.38, 156.51, 167.14, 171.23, 172.95; ESI-MS calculated for $C_{24}H_{20}N_2O_7$ [M+Na]= 471.1163, obs= 471.1187; IR (DMSO) υ 3449, 1736, 1667, 1605, 1566 cm^{-1}.

Synthesis of Compound 1.4

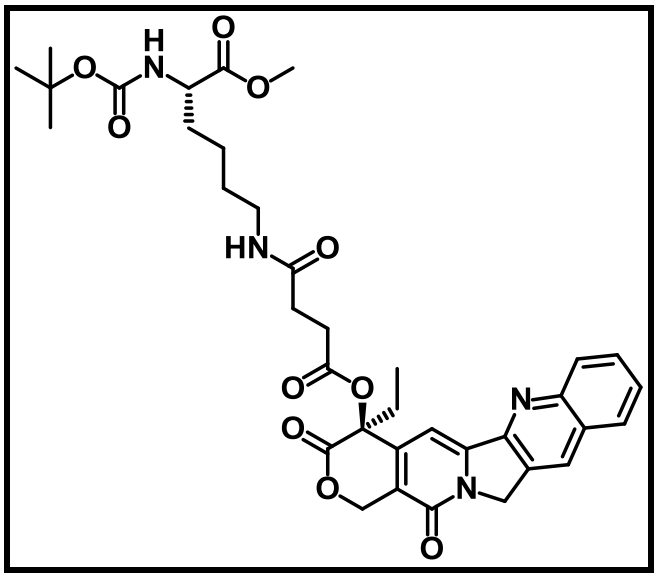

In a 10 mL round bottom flask, **2.1** (0.140 g, 0.3122 mmol), **1.2** (0.162 g, 0.6244 mmol), EDCI (0.120 g, 0.6244 mmol), and DMAP (0.076 g, 0.6244 mmol) were dissolved in DMF (1.56 mL). After stirring for 48 hr, solvent was removed in vacuo and crude was purified via column chromatography (10:1 CH_2Cl_2:MeOH, R_f: 0.86) yielding orange, fluffy solid (165 mg, 77%, m.p. (CH_2Cl_2): 71-74°C). ^{1}H NMR (400 MHz, DMSO) δ 0.90-0.93 (t, 3H, J= 7 Hz), 1.35-1.37 (m, 11H), 1.38-1.90 (m, 2H), 2.15 (m, 2H), 2.38 (m, 2H), 2.59-2.61 (m, 2H), 2.74 (m, 2H), 3.60 (s, 3H), 5.30 (s, 2H) 5.48 (s, 2H), 7.09 (s, 1H), 7.72 (t, 1H, J= 7 Hz), 7.87 (t, 1H, J= 7 Hz), 8.14 (t, 2H, J= 9 Hz), 8.70 (s, 1H); ^{13}C NMR (400 MHz, DMSO) δ 7.50, 22.81, 27.52, 28.10, 28.73, 29.55, 30.22, 30.98, 40.53, 48.55, 51.61, 52.57, 53.47, 66.16, 75.83, 78.04, 78.21, 118.67, 127.68, 128.31, 128.84, 129.69, 130.41, 145.82, 147.81, 152.28, 154.54, 155.64, 156.70, 167.27, 169.88, 171.48, 174.41, 200.17; ESI-MS calculated for $C_{36}H_{42}N_4O_{10}$ [M+H] calc= 691.2974, obs= 691.2964; IR (DMSO) υ 3426, 1744, 1705, 1667, 1620, 1535 cm^{-1}.

Synthesis of Compound 1.0

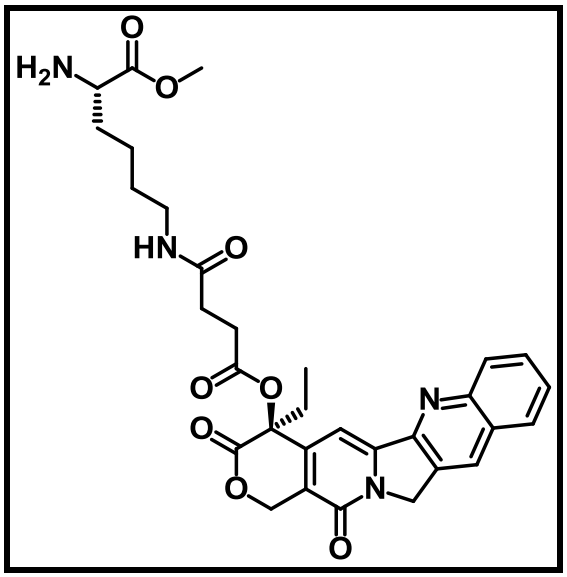

To a 5 mL flask was added 3.1 (40 mg, 0.0580 mmol). The solid was dissolved in CH_2Cl_2 and TFA (0.36 mL) was added dropwise for 1 min. The reaction was stirred for 4 h and then solvent was removed in vacuo. Crude was dissolved in CH_2Cl_2 (5 mL) and solvent evaporated, repeated. Crude was purified by HPLC yielding yellow fluffy solid (26 mg, 76%, m.p.(CH_2Cl/DMSO) 132-135°C: . ^{1}H NMR (400 MHz, DMSO) δ 0.92 (t, 3H, J= 7 Hz),1.21-1.38 (m, 4H), 1.62-1.75 (m, 2H), 2.15 (m, 2H), 2.37 (m, 2H), 2.67-2.83 (m, 2H), 2.90-3.11 (m, 2H), 3.73 (s, 3H), 3.98 (m, 1H), 5.32 (s, 2H), 5.49 (s, 2H), 7.14 (s, 1H), 7.72 (t, 1H, J= 7 Hz), 7.88 (t, 1H, J= 7 Hz), 8.17 (t, 2H, J= 9 Hz), 8.28 (broad s, 2H) 8.72 (s, 1H); ^{13}C NMR (400 MHz, DMSO) δ 7.49, 21.51, 28.35, 228.90, 29.54, 30.25, 50.18, 51.79, 52.73, 58.63, 58.96, 59.29, 66.19, 75.82, 95.28, 118.72, 123.87, 126.65, 127.74, 127.94, 128.81, 129.70, 131.65, 145.83, 147.80, 152.27, 156.57, 167.27, 169.86, 170.19, 171.51; ESI-MS calculated for $C_{31}H_{34}N_4O_8$ [M+H] calc= 591.2449, obs= 591.2448; IR (DMSO) υ 3356, 3201, 1744, 1667, 1604, 1558 cm^{-1}.

Synthesis of Compound 2.0

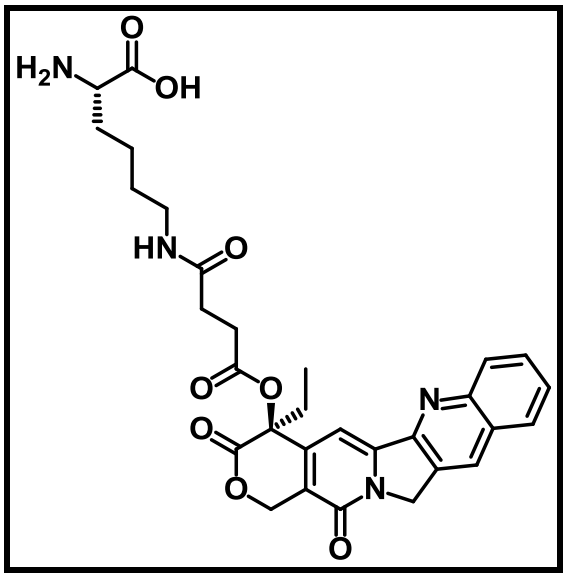

See page 40 for synthesis. Yielded yellow, fluffy solid. (m.p. (H_2O): 138-140 °C). ^{1}H NMR (250 MHz, DMSO) δ 0.92 (t, 3H, J= 7 Hz), 1.23-1.38 (m, 4H), 1.68-1.70 (m, 2H), 2.15 (q, 2H, J= 6 Hz), 2.35 (m, 2H), 2.74 (m, 2H), 3.03 (m, 2H), 3.84 (m, 1H), 5.31 (s, 2H), 5.49 (s, 2H), 7.14 (s, 1H), 7.30 (t, 1H, J= 7H), 7.81 (t, 2H, J= 7Hz), 8.16 (m, 4H), 8.71 (s, 1H); ^{13}C NMR (400 MHz, DMSO) δ 7.53, 16.12, 23.10, 27.26, 28.51, 28.91, 29.62, 30.29, 34.42, 51.79, 57.01, 68.00, 75.85, 95.85, 119.66, 121.57, 126.89, 128.57, 129.61, 131.97, 144.43, 146.02, 156.52, 170.95, 171.11, 177.29, 180.98; ESI-MS calculated for $C_{30}H_{32}N_4O_8$ [M+H] calc= 577.2293, obs= 577.2108; IR (DMSO) υ 3294, 3040, 1751, 1670, 1667, 1612, 1558 cm^{-1}.

Synthesis of Compound 3.0

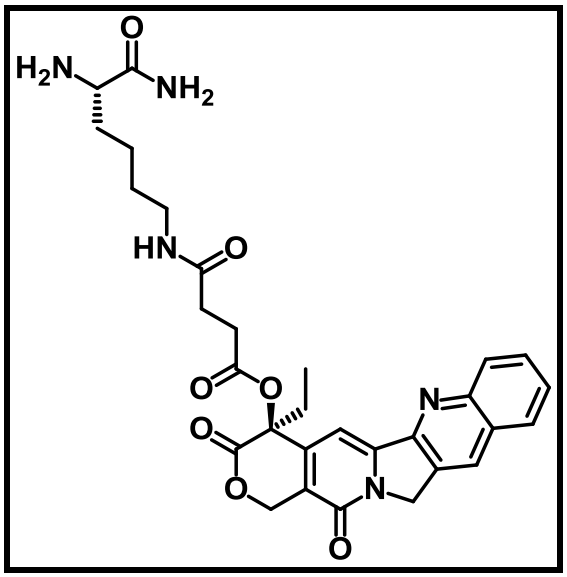

See page 40 for synthesis. Yielded yellow, fluffy solid (m.p. (H_2O): 157-161 °C). ^{1}H NMR (400 MHz, DMSO) δ 0.86 (t, 3H, J= 7 Hz), 1.28-1.31 (m, 2H), 1.55-4.60 (m, 2H), 2.10 (m, 2H), 2.28 (m, 2H), 2.61-2.77 (m, 2H), 2.91-3.02 (m, 2H), 3.56-3.58 (m, 1H), 5.24 (s, 2H), 5.43 (s, 2H), 7.07 (s, 1H), 7.65 (t, 1H, J= 7 Hz), 7.82 (t, 1H, J=7 Hz), 8.10 (t, 2H, J= 9 Hz), 8.64 (s, 1H) ^{13}C NMR (400 MHz, DMSO) δ 7.53, 21.73, 28.63, 28.90, 29.64, 30.34, 30.54, 33.72, 50.42, 52.07, 66.41, 75.82, 95.11, 101.25, 118.80, 127.97, 128.62, 129.03, 129.78, 131.59, 145.39, 145.94, 156.53, 167.25, 170.12, 170.34, 171.61, 173.61; ESI-MS calculated for $C_{30}H_{33}N_5O_7$ [M+H] calc= 576.2453, obs= 576.2460; IR (DMSO) υ 3449, 3302, 3171, 3043, 1751, 1690, 1667, 1612, 1551 cm^{-1}.

References

1. Bardeesy, N.; DePinho, R. A., Pancreatic cancer biology and genetics. *Nat Rev Cancer* **2002,** *2* (12), 897-909.

2. National Cancer Institute, Pancreatic carcinoma. In *A.D.A.M. Medical Encyclopedia*, 2011.

3. American Cancer Society, Cancer Facts & Figures 2012. American Cancer Society: Atlanta, 2012.

4. SEER Survival Monograph: Cancer Survival Among Adults: U.S. SEER Program, 1988-2001, Patient and Tumor Characteristics. Ries LAG, Y. J., Keel GE, Eisner MP, Lin YD, Horner M-J, Ed. National Cancer Institute, SEER Program, NIH: Bethesda, 2007.

5. Rosenberg, L., Pancreatic cancer - A review of emerging therapies. *Drugs* **2000,** *59* (5), 1071-1089.

6. Schnall, S. F.; MacDonald, J. S., Chemotherapy of adenocarcinoma of the pancreas. *Semin Oncol* **1996,** *23* (2), 220-228.

7. Traverso, L. W., Pancreatic cancer: surgery alone is not sufficient. *Surg Endosc* **2006,** *20*, 446-449.

8. Lu, Y. Y.; Jing, D. D.; Xu, M.; Wu, K.; Wang, X. P., Anti-tumor activity of erlotinib in the BxPC-3 pancreatic cancer cell line. *World J Gastroentero* **2008,** *14* (35), 5403-5411.

9. Kindler, H. L.; Friberg, G.; Singh, D. A.; Locker, G.; Nattam, S.; Kozloff, M.; Taber, D. A.; Karrison, T.; Dachman, A.; Stadler, W. M.; Vokes, E. E., Phase II trial of bevacizurnab plus gemcitabine in patients with advanced pancreatic cancer. *J Clin Oncol* **2005,** *23* (31), 8033-8040.

10. Pan, P. S.; Vasko, R. C.; Lapera, S. A.; Johnson, V. A.; Sellers, R. P.; Lin, C. C.; Pan, C. M.; Davis, M. R.; Ardi, V. C.; McAlpine, S. R., A comprehensive study of Sansalvamide A

derivatives: The structure-activity relationships of 78 derivatives in two pancreatic cancer cell lines. *Bioorgan Med Chem* **2009,** *17* (16), 5806-5825.

11. Zamboni, W. C., Concept and clinical evaluation of carrier-mediated anticancer agents. *Oncologist* **2008,** *13* (3), 248-260.

12. Gao, Y.; Yang, Z. M.; Kuang, Y.; Ma, M. L.; Li, J. Y.; Zhao, F.; Xu, B., Enzyme-Instructed Self-Assembly of Peptide Derivatives to Form Nanofibers and Hydrogels. *Biopolymers* **2010,** *94* (1), 19-31.

13. Shao, H.; Parquette, J. R., Controllable Peptide-Dendron Self-Assembly: Interconversion of Nanotubes and Fibrillar Nanostructures. *Angew Chem Int Edit* **2009,** *48* (14), 2525-2528.

14. Keereweer, S.; Mol, I. M.; Kerrebijn, J. D. F.; Van Driel, P. B. A. A.; Xie, B. W.; De Jong, R. J. B.; Vahrmeijer, A. L.; Lowik, C. W. G. M., Targeting integrins and enhanced permeability and retention (EPR) effect for optical imaging of oral cancer. *J Surg Oncol* **2012,** *105* (7), 714-718.

15. Fang, J.; Nakamura, H.; Maeda, H., The EPR effect: Unique features of tumor blood vessels for drug delivery, factors involved, and limitations and augmentation of the effect. *Adv Drug Deliver Rev* **2011,** *63* (3), 136-151.

16. Maeda, H., The enhanced permeability and retention (EPR) effect in tumor vasculature: The key role of tumor-selective macromolecular drug targeting. *Adv Enzyme Regul* **2001,** *41*, 189-207.

17. Godin, B., Serda, R. E., Sakamoto, J., Decuzzi, P. and Ferrari, M, Nanoparticles for Cancer Detection and Therapy. *Nanotechnology* **2010**, 51-88.

18. Torchilin, V. P., Recent advances with liposomes as pharmaceutical carriers. *Nat Rev Drug Discov* **2005,** *4* (2), 145-160.

19. Farrell, J., The Origin of Cancer and the Role of Nutrient Supply - a New Perspective - Abstract. *Med Hypotheses* **1988,** *25* (2), 119-123.

20. Nel, A.; Xia, T.; Madler, L.; Li, N., Toxic potential of materials at the nanolevel. *Science* **2006,** *311* (5761), 622-627.

21. Shvedova, A. A.; Castranova, V.; Kisin, E. R.; Schwegler-Berry, D.; Murray, A. R.; Gandelsman, V. Z.; Maynard, A.; Baron, P., Exposure to carbon nanotube material: Assessment of nanotube cytotoxicity using human keratinocyte cells. *J Toxicol Env Heal A* **2003,** *66* (20), 1909-1926.

22. *Drug Delivery in Oncology: From Basic Research to Cancer Therapy*. Wiley-VCH Verlag & Co. KGaA: Weineim, 2012; Vol. 1.

23. Antonian, L.; Burton, K.; Goodin, R.; Bentley, M.; Eldon, M. A., PEGylation governs the disposition and metabolism of irinotecan following administration of a novel PEG-irinotecan conjugate. *Ejc Suppl* **2007,** *5* (4), 115-115.

24. Schluep, T.; Hwang, J.; Cheng, J. J.; Heidel, J. D.; Bartlett, D. W.; Hollister, B.; Davis, M. E., Preclinical efficacy of the camptothecin-polymer conjugate IT-101 in multiple cancer models. *Clin Cancer Res* **2006,** *12* (5), 1606-1614.

25. Mi, Z. H.; Burke, T. G., Differential Interactions of Camptothecin Lactone and Carboxylate Forms with Human Blood Components. *Biochemistry-Us* **1994,** *33* (34), 10325-10336.

26. Shao, H.; Gao, M.; Kim, S. H.; Jaroniec, C. P.; Parquette, J. R., Aqueous Self-Assembly of L-Lysine-Based Amphiphiles into 1D n-Type Nanotubes. *Chem-Eur J* **2011,** *17* (46), 12882-12885.

27. Numbenjapon, T.; Wang, J. Y.; Colcher, D.; Schluep, T.; Davis, M. E.; Duringer, J.; Kretzner, L.; Yen, Y.; Forman, S. J.; Raubitschek, A., Preclinical Results of Camptothecin-Polymer Conjugate (IT-101) in Multiple Human Lymphoma Xenograft Models. *Clin Cancer Res* **2009,** *15* (13), 4365-4373.

28. Svenson, S.; Wolfgang, M.; Hwang, J.; Ryan, J.; Eliasof, S., Preclinical to clinical development of the novel camptothecin nanopharmaceutical CRLX101. *J Control Release* **2011,** *153* (1), 49-55.

29. Cirpanli, Y.; Bilensoy, E.; Dogan, A. L.; Calis, S., Comparative evaluation of polymeric and amphiphilic cyclodextrin nanoparticles for effective camptothecin delivery. *Eur J Pharm Biopharm* **2009,** *73* (1), 82-89.

30. Wikehooley, J. L.; Haveman, J.; Reinhold, H. S., The Relevance of Tumor Ph to the Treatment of Malignant Disease. *Radiother Oncol* **1984,** *2* (4), 343-366.

31. (a) Li, X. Q.; Wen, H. Y.; Dong, H. Q.; Xue, W. M.; Pauletti, G. M.; Cai, X. J.; Xia, W. J.; Shi, D. L.; Li, Y. Y., Self-assembling nanomicelles of a novel camptothecin prodrug engineered with a redox-responsive release mechanism. *Chem Commun* **2011,** *47* (30), 8647-8649; (b) Norbedo, S.; Dinon, F.; Bergamin, M.; Bosi, S.; Aroulmoji, V.; Khan, R.; Murano, E., Synthesis of 6-amino-6-deoxyhyaluronan as an intermediate for conjugation with carboxylate-containing compounds: application to hyaluronan-camptothecin conjugates. *Carbohyd Res* **2009,** *344* (1), 98-104; (c) Tong, R.; Cheng, J. J., Controlled Synthesis of Camptothecin-Polylactide Conjugates and Nanoconjugates. *Bioconjugate Chem* **2010,** *21* (1), 111-121.

32. Shao, H.; Seifert, J.; Romano, N. C.; Gao, M.; Helmus, J. J.; Jaroniec, C. P.; Modarelli, D. A.; Parquette, J. R., Amphiphilic Self-Assembly of an n-Type Nanotube. *Angew Chem Int Edit* **2010,** *49* (42), 7688-7691.

33. Shao, H.; Nguyen, T.; Romano, N. C.; Modarelli, D. A.; Parquette, J. R., Self-Assembly of 1-D n-Type Nanostructures Based on Naphthalene Diimide-Appended Dipeptides. *J Am Chem Soc* **2009,** *131* (45), 16374-+.

34. (a) Kim, H. J.; Zin, W. C.; Lee, M., Anion-directed self-assembly of coordination polymer into tunable secondary structure. *J Am Chem Soc* **2004,** *126* (22), 7009-7014; (b) Zou, D. W.; Tie, Z. X.; Lu, C. M.; Qin, M.; Lu, X. M.; Wang, M.; Wang, W.; Chen, P., Effects of Hydrophobicity and Anions on Self-Assembly of the Peptide EMK16-II. *Biopolymers* **2010,** *93* (4), 318-329.

35. Wan, W.; Huang, Y.; Wang, Z. Y.; Russell, W. K.; Pai, P. J.; Russell, D. H.; Liu, W. R., A Facile System for Genetic Incorporation of Two Different Noncanonical Amino Acids into One Protein in Escherichia coli. *Angew Chem Int Edit* **2010,** *49* (18), 3211-3214.

36. Isidro-Llobet, A.; Murillo, T.; Bello, P.; Cilibrizzi, A.; Hodgkinson, J. T.; Galloway, W. R. J. D.; Bender, A.; Welch, M.; Spring, D. R., Diversity-oriented synthesis of macrocyclic peptidomimetics. *P Natl Acad Sci USA* **2011,** *108* (17), 6793-6798.

Appendix

^{1}H and ^{13}C NMR

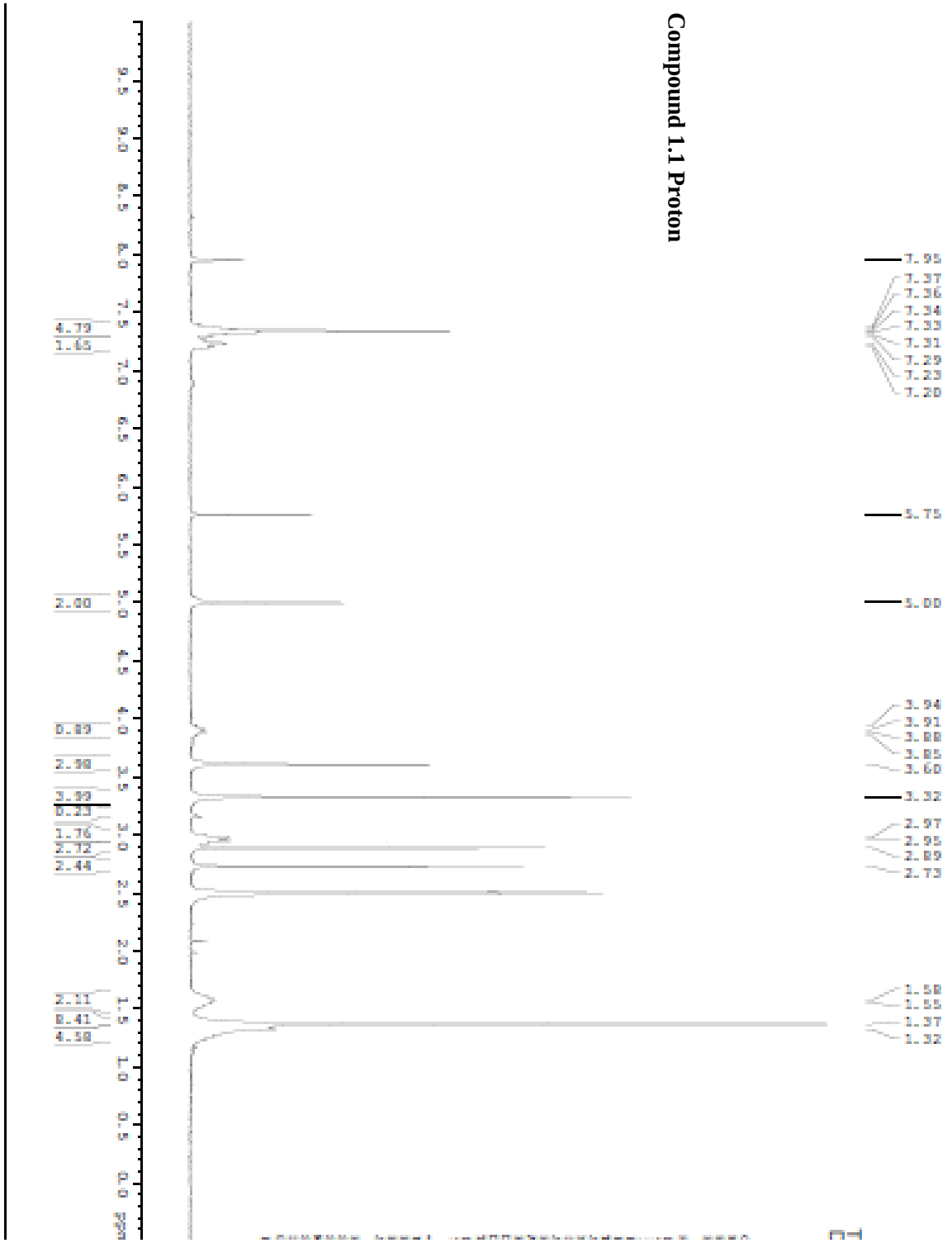

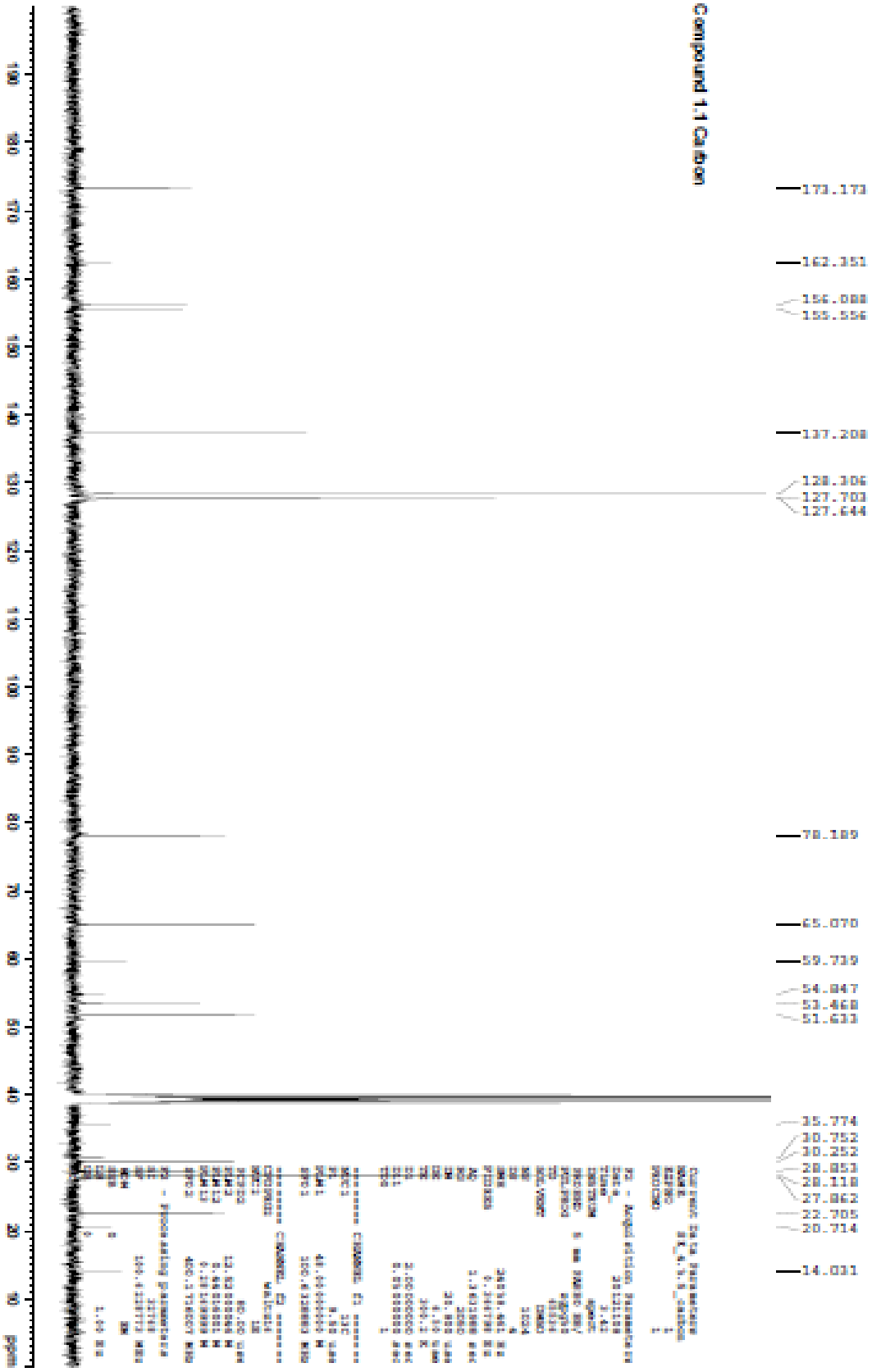
Compound 1.1 Carbon
173.173
162.351
156.088
155.556
137.208
128.306
127.703
127.644
78.189
65.070
59.739
54.847
53.468
51.633
35.774
30.752
30.252
28.853
28.118
27.862
22.705
20.714
14.031
ppm

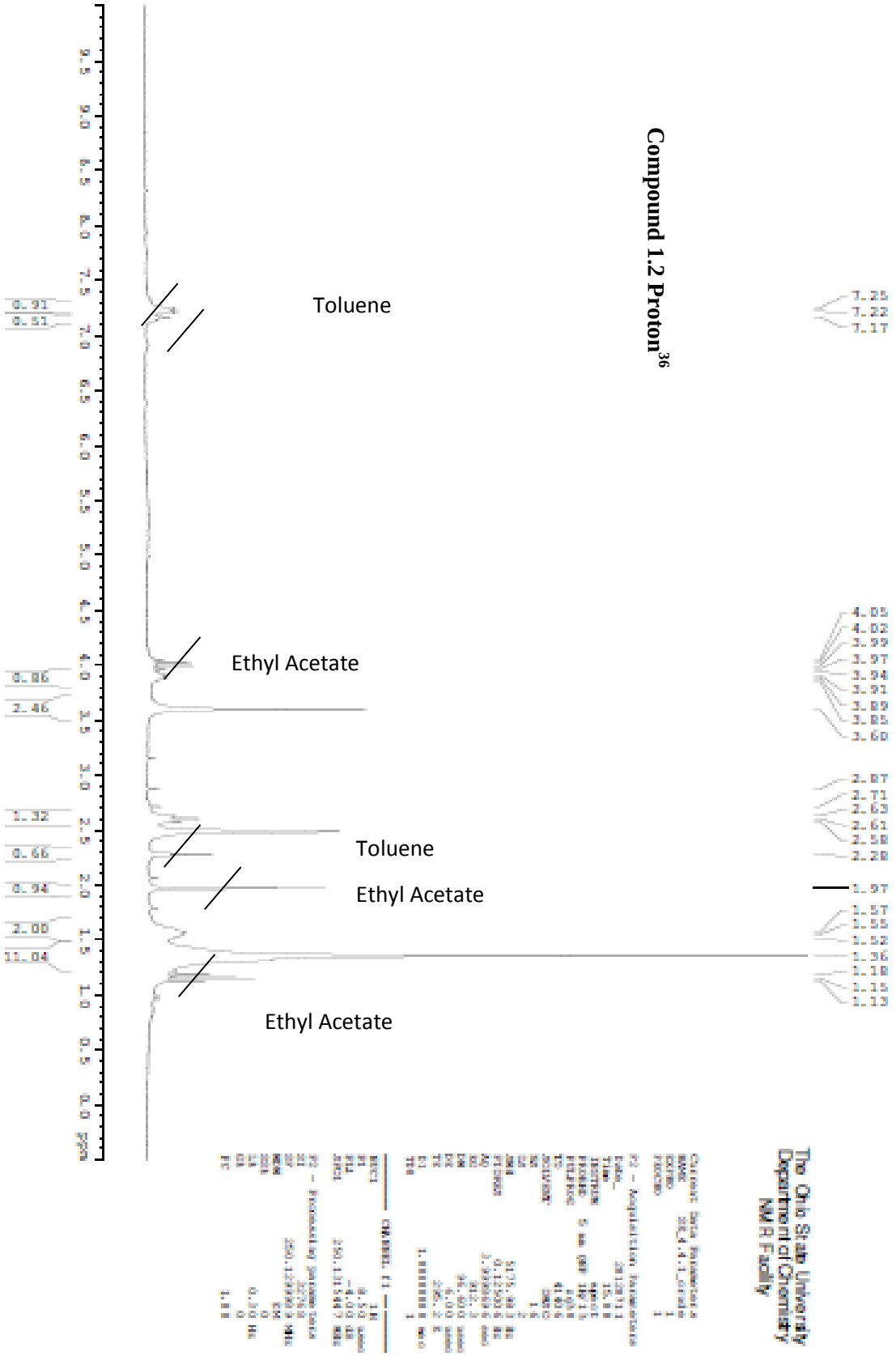
Compound 1.2 Proton[36]
Toluene
Ethyl Acetate
Toluene
Ethyl Acetate
Ethyl Acetate
The Ohio State University
Department of Chemistry
NMR Facility

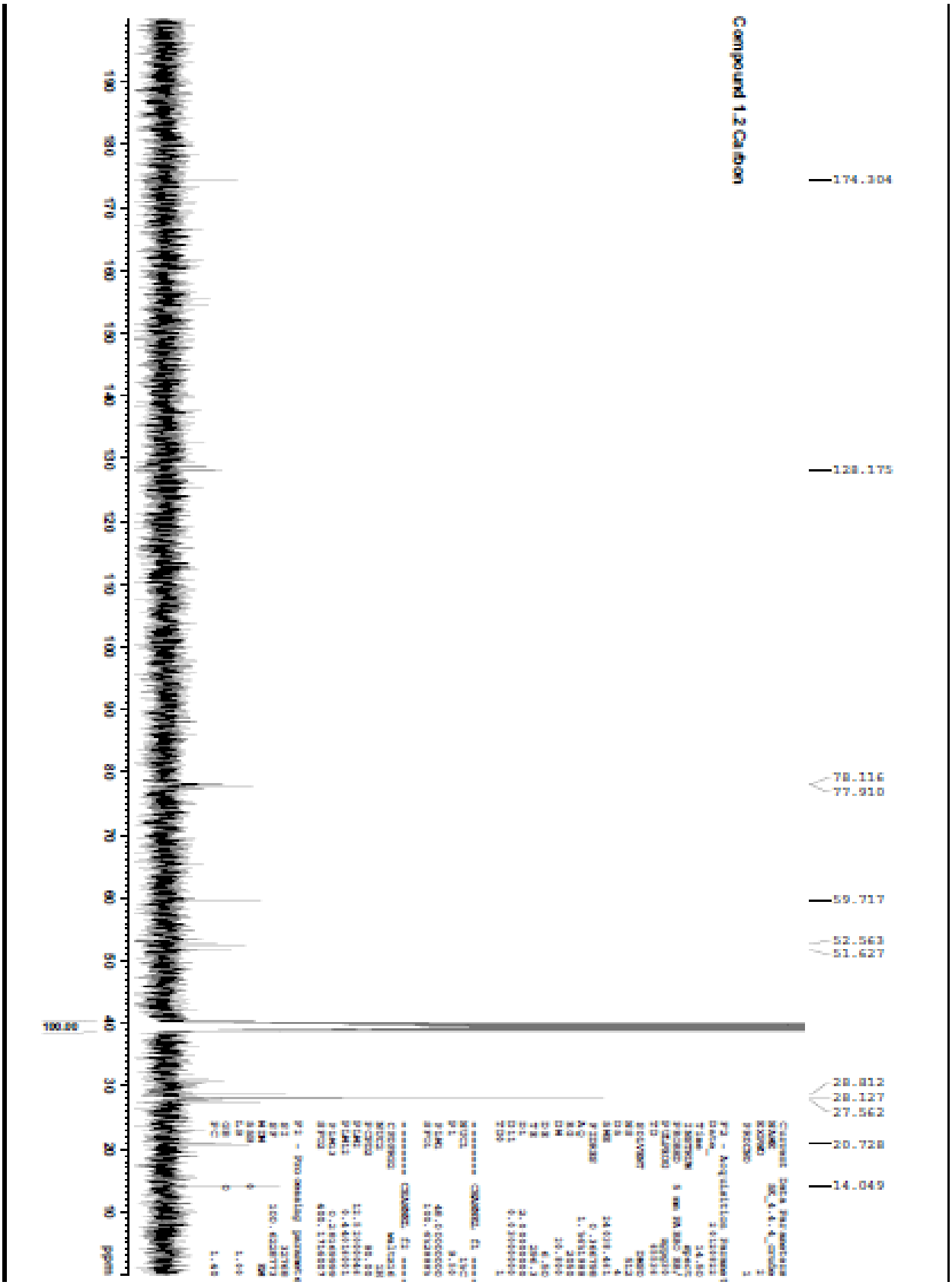
Compound 12 Carbon
174.304
128.175
78.116
77.910
59.717
52.563
51.627
28.812
28.127
27.562
20.728
14.049
100.00
ppm

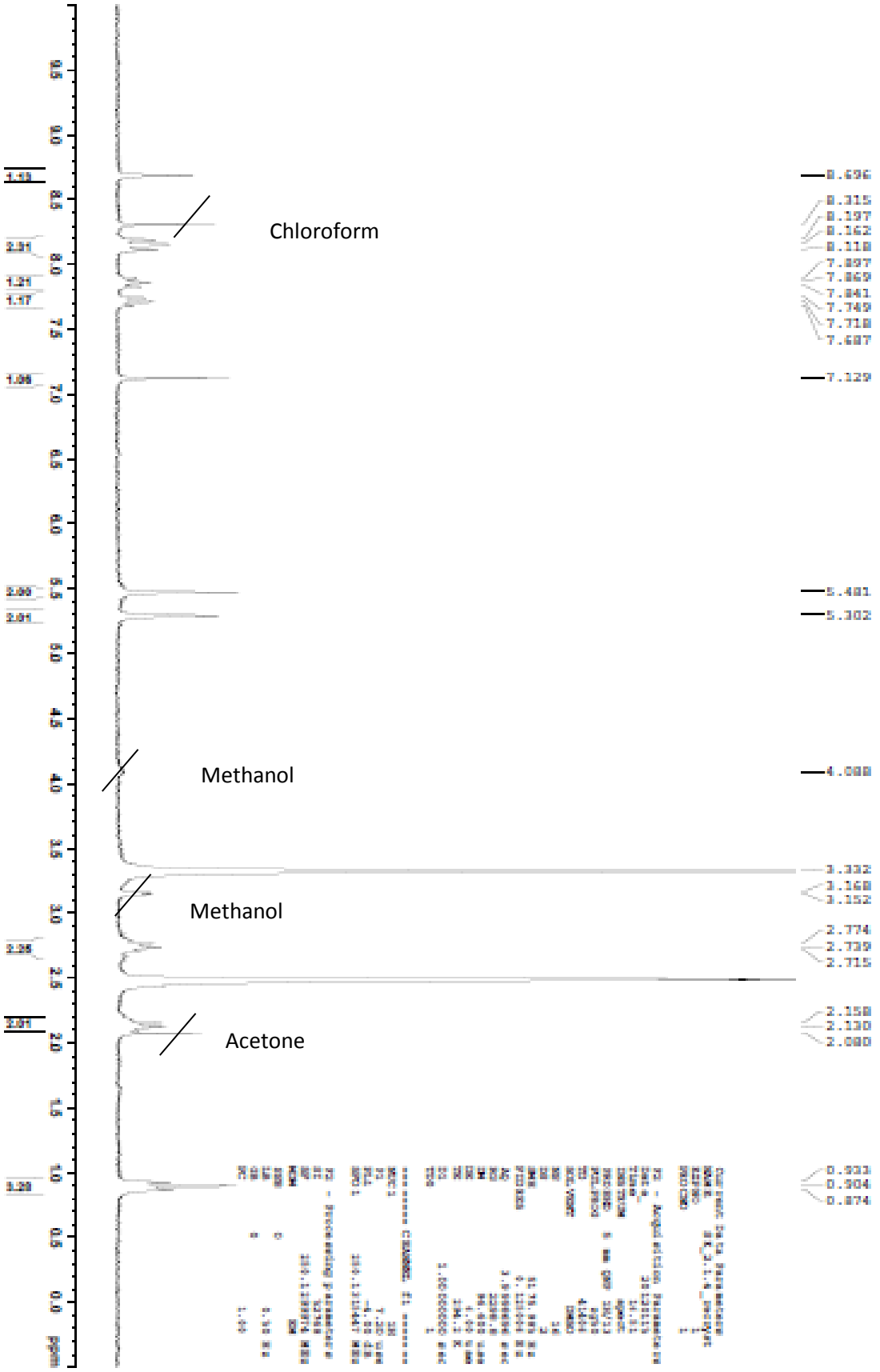
Chloroform
Methanol
Methanol
Acetone
8.696
8.315
8.197
8.162
8.118
7.897
7.869
7.841
7.749
7.718
7.687
7.129
5.481
5.302
4.088
3.332
3.168
3.152
2.774
2.739
2.715
2.158
2.130
2.080
0.933
0.904
0.874

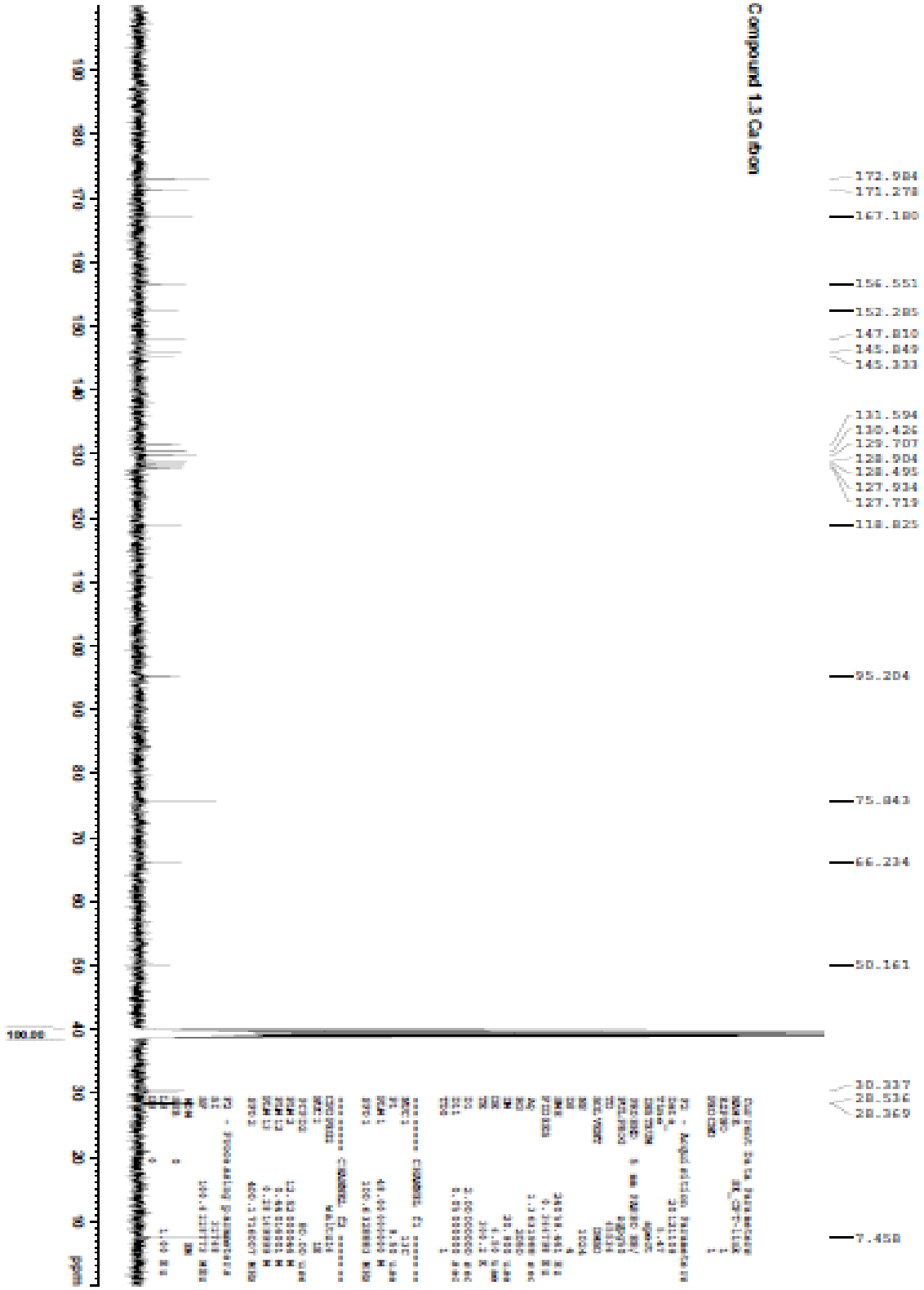
Compound 13 Carbon
172.984
171.278
167.180
156.551
152.285
147.810
145.849
145.333
131.594
130.426
129.707
128.904
128.495
127.934
127.719
118.825
95.204
75.843
66.234
50.161
30.337
28.536
28.369
7.458
100.00

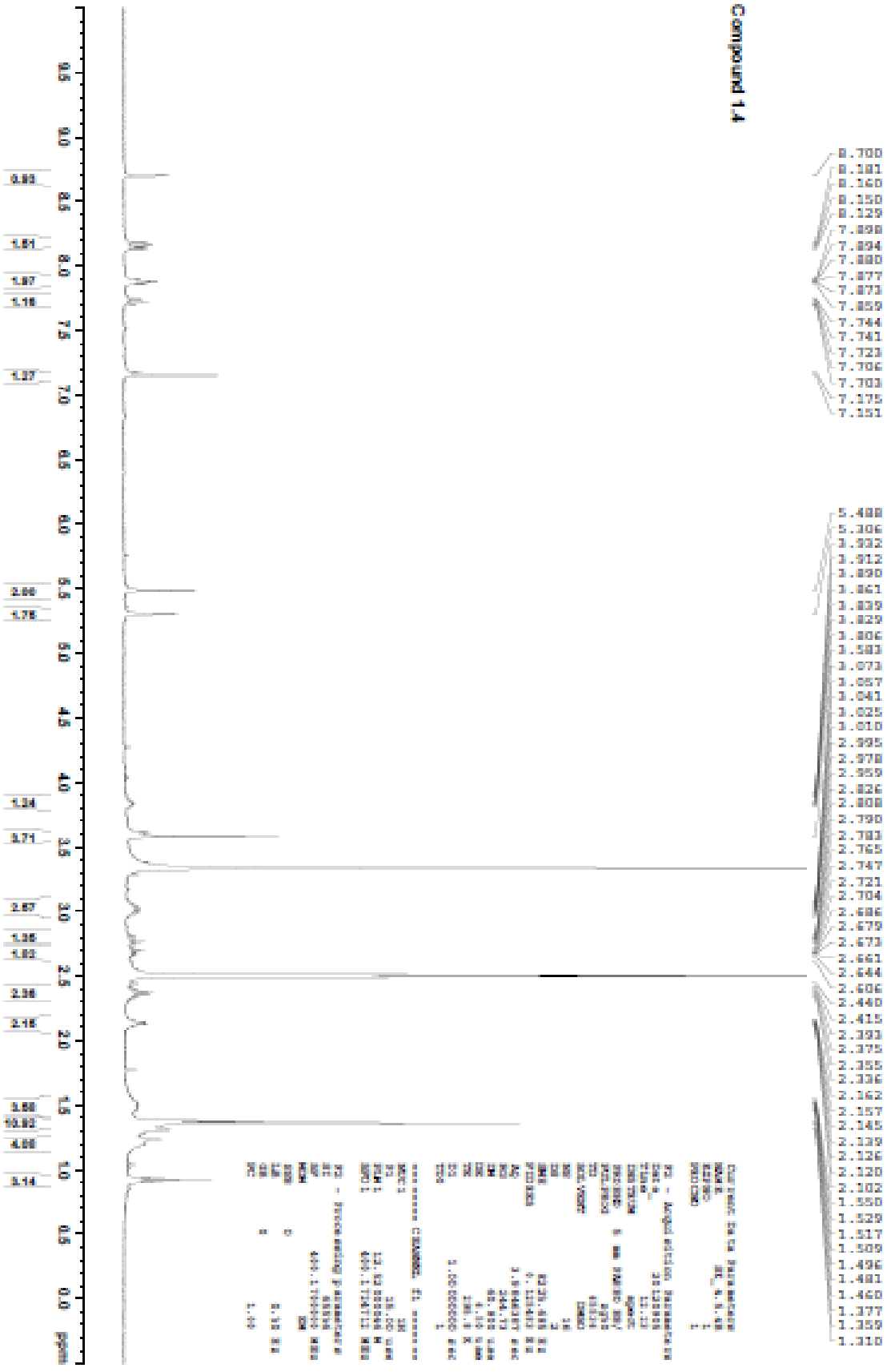
Compound 14
8.700
8.181
8.160
8.150
8.129
7.898
7.894
7.880
7.877
7.873
7.859
7.744
7.741
7.723
7.706
7.703
7.175
7.151
5.488
5.306
3.932
3.912
3.890
3.861
3.839
3.829
3.806
3.583
3.073
3.057
3.041
3.025
3.010
2.995
2.978
2.959
2.826
2.808
2.790
2.783
2.765
2.747
2.721
2.704
2.686
2.679
2.673
2.661
2.644
2.606
2.440
2.415
2.393
2.375
2.355
2.336
2.162
2.157
2.145
2.139
2.126
2.120
2.102
1.550
1.529
1.517
1.509
1.496
1.481
1.460
1.377
1.359
1.310
0.93
1.81
1.87
1.16
1.27
2.00
1.78
1.24
3.71
2.87
1.35
1.02
2.36
2.16
3.50
10.92
4.08
3.14
ppm

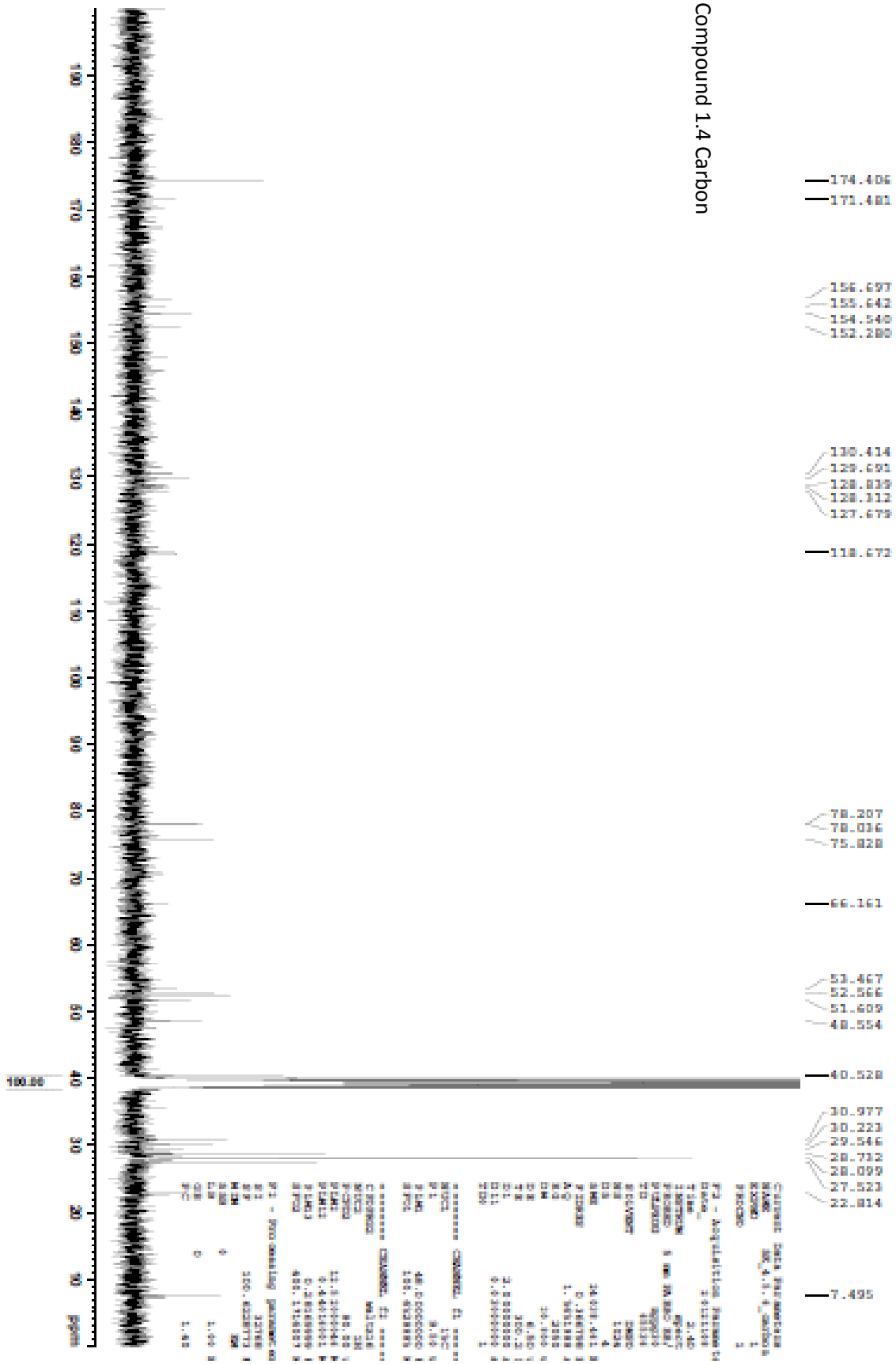
Compound 1.4 Carbon
174.406
171.481
156.697
155.642
154.540
152.280
130.414
129.691
128.839
128.312
127.679
118.672
78.207
78.036
75.828
66.161
53.467
52.566
51.609
48.554
40.528
30.977
30.223
29.546
28.732
28.099
27.523
22.814
7.495

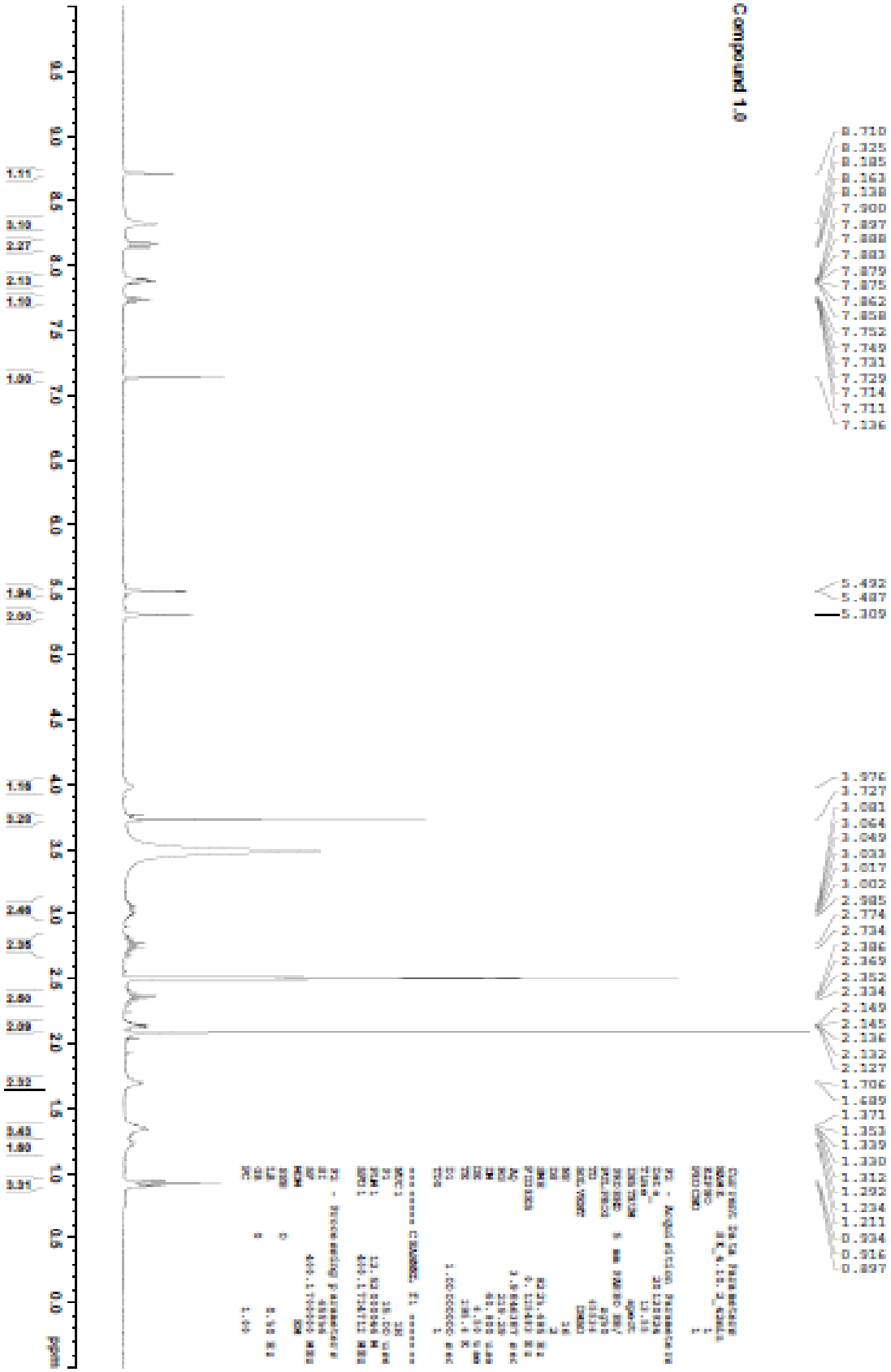
Compound 1.0
8.710
8.325
8.185
8.163
8.138
7.900
7.897
7.888
7.883
7.879
7.875
7.862
7.858
7.752
7.749
7.731
7.729
7.714
7.711
7.136
5.492
5.487
5.309
3.976
3.727
3.081
3.064
3.049
3.033
3.017
3.002
2.985
2.774
2.734
2.386
2.369
2.352
2.334
2.149
2.145
2.136
2.132
2.127
1.706
1.689
1.371
1.353
1.339
1.330
1.312
1.292
1.234
1.211
0.934
0.916
0.897

Compound 1.0 Carbon

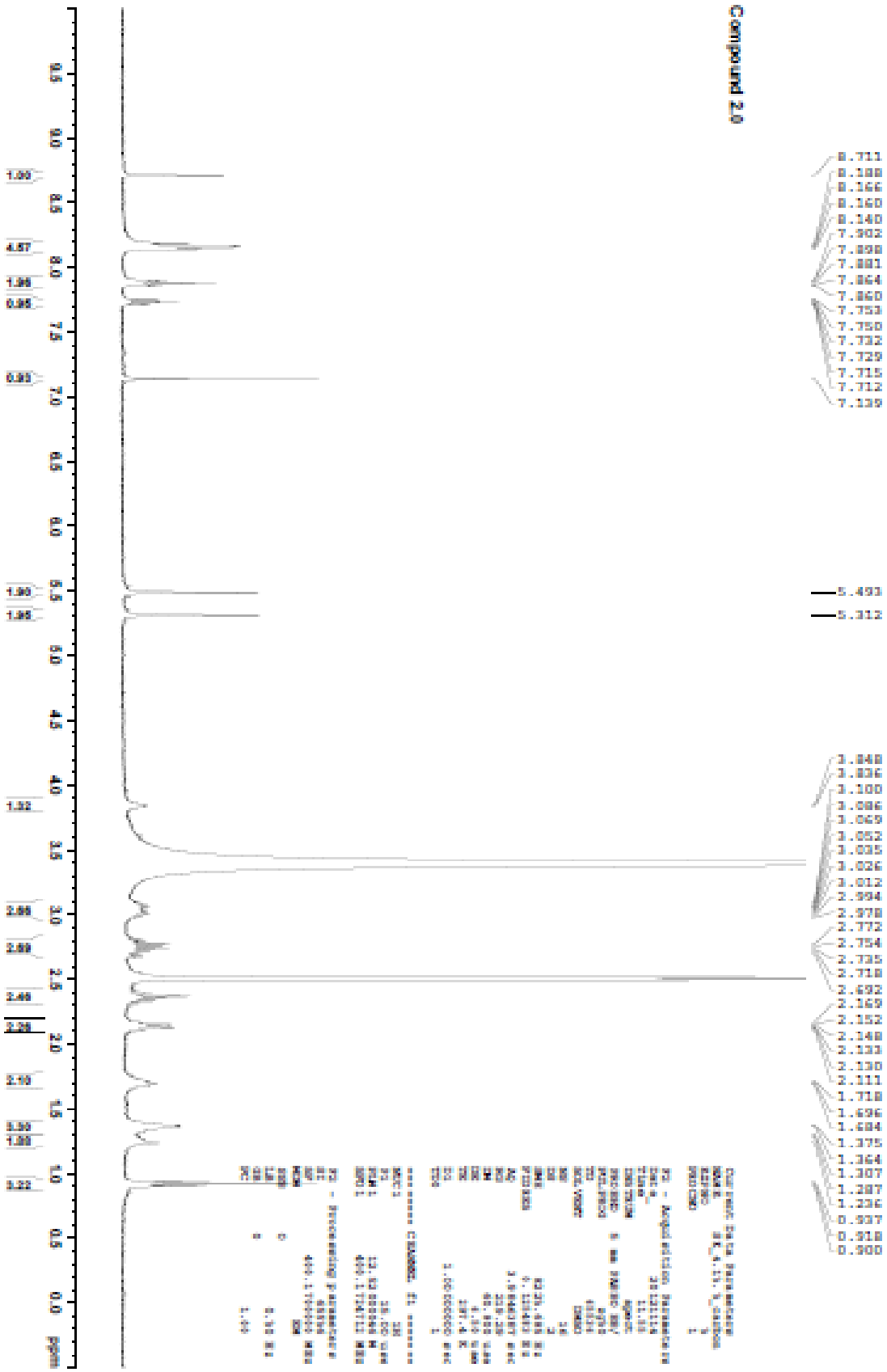
Compound 29
8.711
8.188
8.166
8.160
8.140
7.902
7.898
7.881
7.864
7.860
7.753
7.750
7.732
7.729
7.715
7.712
7.139
5.493
5.312
3.848
3.836
3.100
3.086
3.069
3.052
3.035
3.026
3.012
2.994
2.978
2.772
2.754
2.735
2.718
2.692
2.169
2.152
2.148
2.133
2.130
2.111
1.718
1.696
1.684
1.375
1.364
1.307
1.287
1.236
0.937
0.918
0.900

Compound 2.0 Carbon

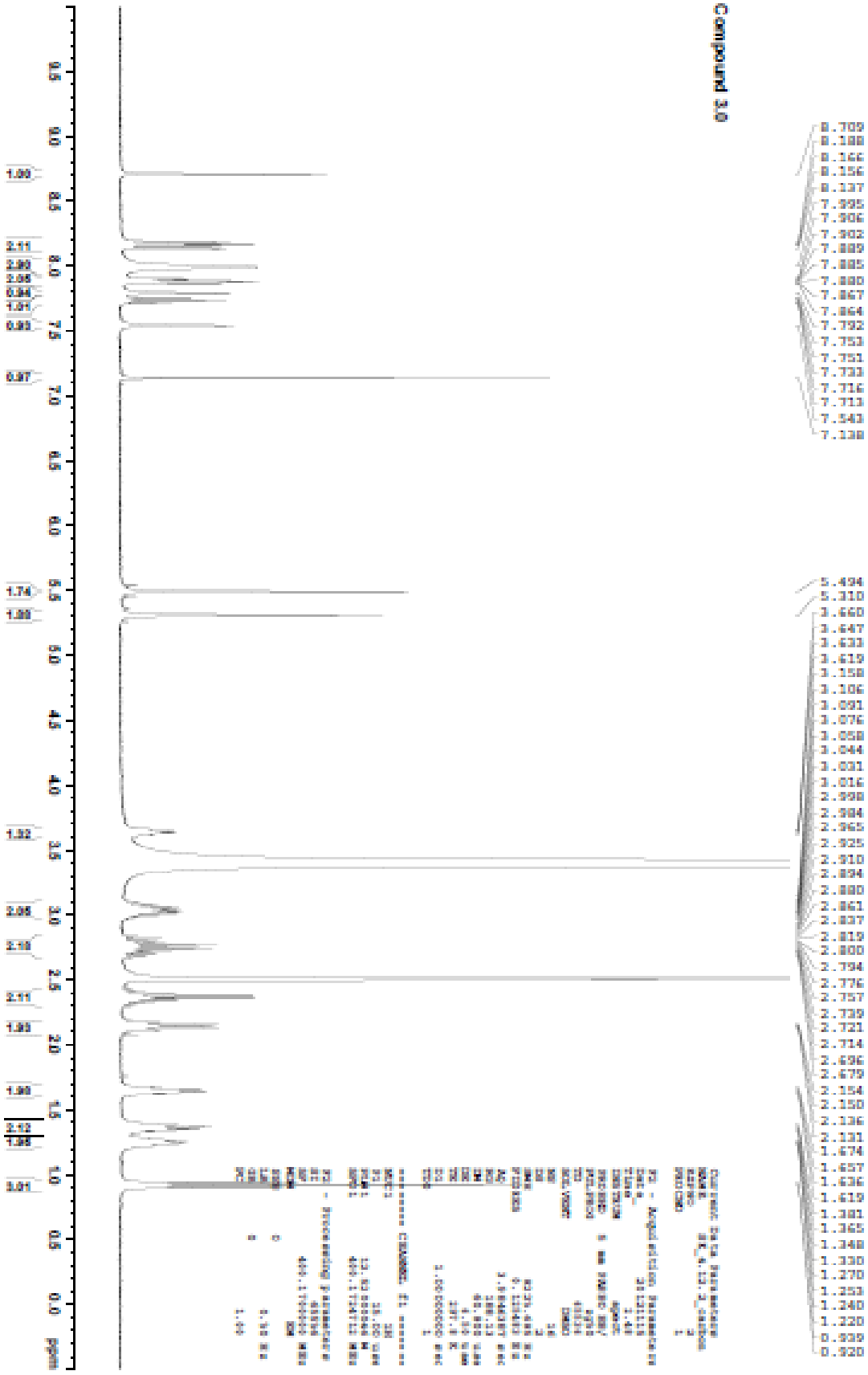
Compound 3.0
8.709
8.188
8.166
8.156
8.137
7.995
7.906
7.902
7.889
7.885
7.880
7.867
7.864
7.792
7.753
7.751
7.733
7.716
7.713
7.543
7.538
5.494
5.310
3.660
3.647
3.633
3.619
3.158
3.106
3.091
3.076
3.058
3.044
3.031
3.016
2.998
2.984
2.965
2.925
2.910
2.894
2.880
2.861
2.837
2.819
2.800
2.794
2.776
2.757
2.739
2.721
2.714
2.696
2.679
2.154
2.150
2.136
2.131
1.674
1.657
1.636
1.619
1.381
1.365
1.348
1.330
1.270
1.253
1.240
1.220
0.939
0.920
1.00
2.11
2.00
2.05
0.94
1.01
0.93
0.97
1.74
1.89
1.32
2.05
2.19
2.11
1.93
1.90
2.12
1.95
3.01
ppm

Compound 3.0 Carbon